



HAL
open science

Timed use of digoxin prevents heart ischemia-reperfusion injury through a REV-ERB α -UPS signaling pathway

Manjula Vinod, Alexandre Berthier, Xavier Maréchal, Céline Gheeraert, Raphaël Boutry, Stéphane Delhaye, Jean-Sébastien Annicotte, Hélène Duez, Agnès Hovasse, Sarah Cianférani, et al.

► To cite this version:

Manjula Vinod, Alexandre Berthier, Xavier Maréchal, Céline Gheeraert, Raphaël Boutry, et al.. Timed use of digoxin prevents heart ischemia-reperfusion injury through a REV-ERB α -UPS signaling pathway. *Nature Cardiovascular Research*, 2022, pp.990-1005. 10.1038/s44161-022-00148-z . inserm-03859910

HAL Id: inserm-03859910

<https://inserm.hal.science/inserm-03859910>

Submitted on 18 Nov 2022

HAL is a multi-disciplinary open access archive for the deposit and dissemination of scientific research documents, whether they are published or not. The documents may come from teaching and research institutions in France or abroad, or from public or private research centers.

L'archive ouverte pluridisciplinaire **HAL**, est destinée au dépôt et à la diffusion de documents scientifiques de niveau recherche, publiés ou non, émanant des établissements d'enseignement et de recherche français ou étrangers, des laboratoires publics ou privés.

7
8
9
10
11
12
13
14
15
16
17
18
19
20
21
22
23
24
25
26
27
28
29

**Timed use of digoxin prevents heart ischemia-reperfusion injury
through a REV-ERB α -UPS signaling pathway**

Manjula Vinod ¹, Alexandre Berthier ¹, Xavier Maréchal ¹, Céline Gheeraert ¹, Raphaël Boutry ²,
Stéphane Delhaye ¹, Jean-Sébastien Annicotte ², Hélène Duez ¹, Agnès Hovasse ³, Sarah Cianférani ³,
David Montaigne ¹, Jérôme Eeckhoutte ¹, Bart Staels ¹, Philippe Lefebvre ^{1,*}

¹ Univ. Lille, Inserm, CHU Lille, Institut Pasteur de Lille, U1011-EGID, F-59000 Lille, France

² Univ. Lille, Inserm, CHU Lille, Institut Pasteur de Lille, U1167 – RID-AGE - Facteurs de risque et
déterminants moléculaires des maladies liées au vieillissement, F-59000 Lille, France

³ Laboratoire de Spectrométrie de Masse BioOrganique (LSMBO), IPHC, Université de Strasbourg,
CNRS, UMR7178, 25 Rue Becquerel, F-67087 Strasbourg, France

* Corresponding author: philippe-claude.lefebvre@inserm.fr

UMR 1011, Bâtiment J&K, Faculté de Médecine de Lille-Pôle Recherche
Boulevard du Professeur Leclerc, 59045 Lille cedex, France
Tel +33.3.20974220

30

31

32

33

34

35

ABSTRACT

36 Myocardial ischemia-reperfusion injury (MIRI) induces life-threatening damages to the cardiac tissue
37 and pharmacological means to achieve cardioprotection are sorely needed. MIRI severity varies along
38 the day-night cycle and is molecularly linked to components of the cellular clock including the nuclear
39 receptor REV-ERB α , a transcriptional repressor. Here we show that digoxin administration in mice is
40 cardioprotective when timed to trigger REV-ERB α protein degradation. In cardiomyocytes, digoxin
41 increases REV-ERB α ubiquitylation and proteasomal degradation, which depend on REV-ERB α ability
42 to bind its natural ligand, heme. Inhibition of the membrane-bound Src tyrosine-kinase partially
43 alleviated digoxin-induced REV-ERB α degradation. In untreated cardiomyocytes, REV-ERB α proteolysis
44 is controlled by several E3 ubiquitin ligases and the proteasome subunit PSMB5. Among these, only
45 SIAH2 and PSMB5 contributed to digoxin-induced degradation of REV-ERB α . Thus, controlling REV-
46 ERB α proteostasis through the ubiquitin-proteasome system is an appealing cardioprotective strategy.
47 Our data support the timed use of clinically-approved cardiotonic steroids in prophylactic
48 cardioprotection.

50 The mammalian circadian clock is a critical cell-autonomous mechanism regulating many, if
51 not all, aspects of cellular, tissular and organismal homeostasis¹. Heart physiology makes no exception
52 to this rule and electrophysiological, mechanical and metabolic functions of the cardiac tissue are
53 submitted to cyclic daily variations², which are dependent on the integrity of the molecular clock³.
54 Quite expectedly, genetic or environmental perturbations of the circadian clock in mouse models lead
55 to cardiovascular pathologies including impaired cardiac contractility, fibrosis and cardiomyopathy.
56 Human observational studies also largely concur to demonstrate that circadian rhythm misalignments
57 are associated with cardiometabolic diseases⁴. The prevalence of adverse cardiovascular events such
58 as stroke and myocardial infarction at the sleep-to-wake transition underlines the complex interplay
59 between (mechanisms of) timed cyclic blood pressure control, heart function and vascular tone
60 regulation. In addition to altering heart responsiveness to pathological events, circadian
61 (dys)regulations also affect the heart and cardiomyocyte's ability to recover from acute injury.

62 Susceptibility to myocardial ischemia-reperfusion injury (MIRI) relies on transient adaptative
63 mechanisms to hypoxia and rapid restoration of oxidative metabolism and contractile efficiency⁵.
64 During ischemia, the myocardial tissue undergoes ATP depletion, acidosis by accumulation of lactic
65 acid and activation of a series of immediate- and late- response intracellular signaling pathways called
66 "RISK" and "SAFE" pathways. These signaling pathways, which are also stimulated upon
67 preconditioning (PC), protect mitochondrial function⁶. Reperfusion causes massive cellular production
68 of reactive oxygen species, alkalinization and calcium overload⁷. Sensitivity to MIRI is time-of-the-day
69 (ToD)-dependent and is exacerbated during the sleep-to-wake transition in human and mouse⁸.
70 Genetic alteration of circadian rhythmicity in mice⁸ or circadian rhythm (dys)synchrony in humans
71 correlate with increased acute cardiac injury⁹. We recently demonstrated that timed antagonism of
72 the cyclically-expressed nuclear receptor REV-ERB α , a heme-binding transcriptional repressor within
73 the molecular clock machinery, preventively protects mouse heart from deleterious effects of MIRI in
74 a p21-dependent manner¹⁰. This observation mechanistically linked the ToD dependency of MIRI with
75 the core clock gene machinery, identifying REV-ERB α as a novel target in pharmacological PC.

76 The search for pharmacologically protective compounds in MIRI has proven difficult¹¹. Despite
77 their continued use in atrial fibrillation to ameliorate heart contractile properties, cardiotonic steroids
78 (CTS) such as digoxin are not recommended in MIRI cardioprotection at therapeutic concentrations¹².
79 Renewed interest in CTS has however sparked from the identification of dissociated inotropic and
80 non-ion pumping signaling properties of Na⁺-K⁺ ATPase (NKA), a target of CTS. Isoforms of the 3 NKA
81 subunits [α , β and γ /FXVD] associate to make up the heteromeric membrane NKA complex. Inotropic

82 effects of CTS are essentially mediated by their ability to bind to and inhibit NKA ATPase activity ¹³,
83 thereby triggering intracellular accumulation of Na⁺ and decreasing Ca⁺⁺ efflux through the Na⁺/Ca⁺⁺
84 exchanger NCX1. CTS-induced signaling responses can be induced at ATPase sub-inhibitory
85 concentrations and stems at least in part from NKA's ability to act as a CTS plasma membrane receptor
86 ^{14,15}. CTS binding to the NKA α 1 subunit allows the activation of multiple downstream intracellular
87 signaling pathways, including part of RISK or SAFE pathways, hence suggesting a potential usefulness
88 of CTS in preventive MIRI protection ¹⁶.

89 Thus, given the temporal gating of signaling pathways, the involvement of both the NKA
90 signalosome and REV-ERB α in MIRI protection, and the known susceptibility of REV-ERB α activity to
91 intracellular signaling pathways, we investigated whether CTS-induced signaling pathways could alter
92 REV-ERB α functions and sensitivity to MIRI. Here we show that digoxin and other CTS activate signaling
93 pathways in cardiomyocytes and trigger REV-ERB α protein degradation through the ubiquitin-
94 proteasome system (UPS) in an SRC kinase-dependent manner. Timed in vivo treatment with digoxin
95 prevented REV-ERB α protein accumulation and conferred protection against MIRI.

96

RESULTS

97

98

99 **Cardioprotection by digoxin is time of the day-dependent.**

100 We previously demonstrated, using the Langendorff heart perfusion model, that isolated
101 mouse hearts display a ToD-dependent sensitivity to MIRI. Mouse hearts are intrinsically more
102 resistant to MIRI at the beginning of the rest phase [zeitgeber time 0 (ZT0), beginning of the light phase]
103 than at the end of this period (ZT12, average infarct size 27% vs 47%)⁽¹⁰⁾ and **Fig. 1a**). We asked whether
104 ex vivo PC efficiency follows a similar pattern. Submitting ZT0 isolated hearts to a short iterative
105 ischemia-reperfusion sequence (PC) prior to a prolonged ischemic period neither protected nor
106 aggravated infarct size. In contrast, MIRI-prone ZT12 hearts were protected by this local PC protocol
107 (average infarct size 31% vs 47%) (**Fig. 1a**). To shed light on these differential sensitivities, the
108 transcriptomic phenotype of ZT0 and ZT12 hearts was investigated (**Fig. 1b** and **Supplementary Dataset**
109 **1**). Only a few protein-encoding genes were found to be differentially expressed (n=145, **Fig. 1b**), with
110 10-12% being core circadian genes including REV-ERB α , which is lowest expressed at ZT0. In addition,
111 \approx 75% of differentially expressed genes are cyclically expressed with a period of 20-24 hours
112 (**Supplementary Dataset 1, Fig. 1b, right panel** and **Fig. 1c**). None of them belonged to RISK or SAFE
113 cardioprotective pathways. Thus, ZT12 hearts are intrinsically more sensitive to MIRI, responsive to
114 PC and exhibit specific molecular phenotypic features related to molecular clock-driven processes.

115 We then assessed whether the previously reported ex vivo PC properties of digoxin can
116 translate in vivo and whether they are ToD-dependent. We injected a single bolus of digoxin 4 hours
117 prior to organ sampling at ZT0 or ZT9 at a pharmacologically well-tolerated dose (1 mpk IP¹⁷). This
118 timing is based on pharmacokinetics studies of digoxin in rodents showing plasma concentration
119 peaking within 1 hour after injection, followed by a 4- to 6-hour tissue distribution phase¹⁸ yielding an
120 estimated extracellular fluid concentration of about 5-10 μ M¹⁹. The infarct size in untreated mice was
121 as in **Fig. 1a**, larger by 20% at ZT9 when compared to ZT0 hearts (**Fig. 1d**), in agreement with¹⁰.
122 Whereas digoxin pretreatment showed a clear, albeit non-significant (p=0.08) trend to increase MIRI
123 at ZT0, it significantly reduced infarct size by 20% at ZT9 (**Fig. 1d**). Pre-ischemic monitoring of heart
124 performances with a constant flow perfusion did not reveal significant changes in contraction force,
125 perfusion pressure and myocardial contractility (**Supplementary Fig. 1a-d**), thus ruling out an effect of
126 digoxin treatment on coronary vascular tone, endothelial function as well as on systolic and diastolic
127 dynamics. In the MIRI model, a significant proportion of hearts displayed post-ischemic ventricular
128 arrhythmias, making the analysis of cardiac contractile performance upon recovery infeasible.

129

130 **Cardioprotection by digoxin is REV-ERB α -dependent.**

131 Since the selected time points correspond to the nadir (ZT0) and zenith (ZT9) of REV-ERB α
132 protein level, respectively (Fig. 1e and Extended data Fig. 1a), we assessed whether digoxin treatment
133 affects REV-ERB α mRNA and protein levels. Increasing doses of digoxin administered at ZT5 led to a
134 dose-dependent decrease REV-ERB α protein level at ZT9 to reach 60% at 1 mpk (Fig. 1f and Extended
135 data Fig. 1b). In contrast, the expression of the REV-ERB α -encoding *Nr1d1* gene, whose expression
136 precedes REV-ERB α protein expression by approximately 2 hours (Fig. 1c and Extended data Fig. 1c),
137 was not affected by digoxin treatment. The expression of REV-ERB α target genes (*Arntl/Bmal1* and
138 *Cdkn1a/p21*, Extended data Fig. 1c), which mirror the REV-ERB α protein level pattern in homeostatic
139 conditions (Fig. 1c and Extended data Fig. 1c), were increased by digoxin treatment (Extended data Fig.
140 1d) as well as P21 protein levels (Extended data Fig. 1e). Digoxin did not affect REV-ERB α protein level
141 at ZT0, which was barely detectable at this time point (Extended data Fig. 1f). This ToD sensitivity to
142 digoxin was not due to changing levels during the day/night cycle of NKA isoforms *ATP1A1*, or *ATP1A2*
143 and *ATP1A3* mRNAs or of corresponding protein levels at the time of treatment (Extended data Fig.
144 2a,b). Their expression was neither affected by REV-ERB α KO (Supplementary Dataset 2) nor by digoxin
145 treatment (Extended data Fig. 2a). Thus, these data suggest that digoxin interferes with REV-ERB α
146 protein levels through post-transcriptional regulation.

147 Digoxin administered at ZT4 did not protect mouse hearts from MIRI at ZT9 in *Nr1d1*^{-/-} mice
148 but rather increased infarct size (+11%) (Fig. 1g), phenotypically mimicking ZT0 hearts (Fig. 1d). REV-
149 ERB α via p21 expression contributes to increased resistance to MIRI¹⁰. A similar experiment in p21-
150 depleted mice confirmed the higher susceptibility of these mice to MIRI but digoxin treatment was still
151 protective in these mice (-18%, average infarct size 55%)(Fig. 1g). Thus, REV-ERB α expression is
152 required to confer cardioprotective properties to a prophylactic digoxin treatment without involving
153 the anti-apoptotic protein P21.

154 Injected digoxin preferentially accumulates in skeletal muscles, heart and liver²⁰. Similar to
155 the cardiac tissue, digoxin-exposed livers displayed reduced REV-ERB α protein level and increased
156 target gene expression (*E4bp4/Nfil3*, *Bmal1/Arntl*, *cdkn1a/p21*), while *Nr1d1* mRNA levels were left
157 unchanged (Supplementary Fig. 2a-e). These observations raised the question of how digoxin
158 downregulates REV-ERB α protein expression.

159

160 **Digoxin affects REV-ERB α proteostasis in a cell-autonomous manner.**

161 Analysis of bulk cardiac tissue as above may overlook outcomes stemming from multiple inter-
162 or intracellular crosstalks. We therefore asked whether REV-ERB α protein degradation occurs in
163 isolated digoxin-treated cardiomyocytes. We first performed experiments using the human
164 cardiomyocyte cell line AC16 from adult human ventricular heart tissue²¹. Since digoxin and other CTS
165 have significant pro-apoptotic properties²², we investigated whether digoxin induces AC16 cell death.
166 AC16 cells were synchronized at T₋₂ by a dexamethasone pulse (2 hours) which transiently induces *Per1*
167 gene expression²³ and subsequently incubated with digoxin at T₀. Cell viability was only mildly affected
168 by digoxin at tested concentrations (Extended data Fig. 3a). Probing apoptosis-related protein levels
169 in AC16 whole cell extracts did not reveal any significant change in the apoptotic cascade (Extended
170 data Fig. 3b). In these conditions, REV-ERB α reached a maximal expression 24 hours after
171 synchronization (T₂₄). Digoxin blunted REV-ERB α expression at all time-points (Fig. 2a and Extended
172 data Fig. 3c). REV-ERB α protein levels were normalized to HSP90 α levels, whose half-life is 36-40
173 hours, vs 1 hour for REV-ERB α . NKA subunits α 1 and α 2 mRNAs and protein levels were steadily
174 detectable in these conditions (Extended data Fig. 2c,d). Digoxin's effect on REV-ERB α protein level
175 was fully prevented by an anti-digoxin antibody (Extended data Fig. 3d), excluding any artifactual
176 modulation of cellular pathways by contaminants. The digoxin effect was dose-dependent with an
177 observed EC₅₀= 96nM (Extended data Fig. 3e), which fits with the reported binding constant of digoxin
178 to the human NKA α 1 subunit (K_D=87nM), the major CTS signalosome relay^{24,25}. It is also consistent
179 with the observed efficiency of the non-glycosylated CTS bufalin [EC₅₀<0.1 μ M (Extended data Fig. 3f),
180 K_D=42nM²⁴]. The structurally-related ouabain also decreased REV-ERB α stability (Extended data Fig.
181 3g).

182 Under basal conditions, expression levels of *NR1D1* and of the REV-ERB α target gene
183 *ANRTL/BMAL1* showed, as expected, an antiphasic transcript expression in untreated AC16 cells (Fig.
184 2b). Digoxin increased at T₂₄ both *NR1D1* and *ANRTL/BMAL1* mRNAs, both known to be directly and
185 cyclically repressed by REV-ERB α (Fig. 2b) and *ANRTL/BMAL1* promoter activity became acyclic (Fig.
186 2c). P21 protein level increased upon digoxin treatment (Fig. 2D), alike after in vivo digoxin injection
187 (Extended data Fig. 1e).

188 Digoxin's effect was also assessed using the human osteosarcoma U2OS cell line, a commonly
189 used and robust circadian model (Extended data Fig. 4a-c). REV-ERB α expression peaked 16-20 hours
190 after synchronization, and digoxin blunted REV-ERB α protein level at all time-points (Extended data
191 Fig. 4a). The expression of ROR α , a transactivator counteracting REV-ERB α activity, remained
192 unchanged (Extended data Fig. 4a) whereas *NR1D1* and *BMAL1/ARNTL* transcripts were higher
193 expressed (Extended data Fig. 4b), with *ANRTL/BMAL1* promoter activity becoming acyclic (Extended
194 data Fig. 4c). Similar results were obtained using human primary cardiomyocytes (Fig. 3) and HepG2

195 cells (Supplementary Fig. 2f). Thus, CTS strongly decrease REV-ERB α protein level in several
196 representative cardiomyocyte models and unrelated cell lines (U2OS, HepG2), suggesting a highly
197 conserved mechanism involving NKA.

198

199 **Digoxin induces multiple intracellular signaling pathways.**

200 Digoxin's effect on REV-ERB α levels are detected after a short treatment (210 minutes,
201 Extended data Fig. 3h). Therefore, digoxin (at 5x EC₅₀=0.5 μ M) and other modulators were, in further
202 experiments, added at T₁₈, 6 hours prior to the REV-ERB α protein peak in order to minimize secondary
203 responses to treatment(s) (Fig. 4a, top panel). In these conditions, we assessed the involvement of
204 NKA as a bifunctional protein regulating ion fluxes and exerting signaling functions, as the calculated
205 in vivo concentration of digoxin (5-10 μ M, Fig. 1d) activates the signalosome-related PKC ϵ in mouse
206 heart²⁶. In vitro, 3,4,5,6 tetrahydroxyxanthone (THX) inhibits NKA ATPase activity with an efficiency
207 similar as ouabain (EC₅₀=1.6 μ M), while being unable to activate Src²⁷. We therefore compared the
208 activity of THX to that of digoxin on REV-ERB α stability. In contrast to digoxin, THX treatment did not
209 alter REV-ERB α levels in AC16 (Fig. 4a and Supplementary Fig. 3a) and U2OS cells (Supplementary Fig.
210 3b), suggesting that the ion pumping activity of NKA is dispensable for digoxin-induced REV-ERB α
211 decrease. Pharmacological perturbation of calcium fluxes through inhibition of voltage-dependent
212 Ca⁺⁺ channels by diltiazem and verapamil (Supplementary Fig. 3c), through SERCA inhibition by
213 thapsigargin (Supplementary Fig. 3d) or through blockade of the Na⁺-Ca⁺⁺ exchange system NCX by KB-
214 R7943 (Supplementary Fig. 3e) did not regulate REV-ERB α protein levels. Taken together, this data
215 rules out a contribution of the inotropic arm of NKA.

216 The ability of digoxin to trigger intracellular pathways at low and moderate concentrations
217 (0.5 μ M and 5.0 μ M) was thus evaluated using serine/threonine (S/T) kinase arrays (Fig. 4b-d). Digoxin
218 activated multiple S/T kinases belonging mostly to the human CMGC (Cyclin-dependent kinases,
219 Mitogen-activated protein kinases, Glycogen synthase kinases, CDC-like kinases), CAMK (Calcium and
220 Calmodulin-regulated Kinases) and the related AGC (PKA, PKG, PKCs) groups (Fig. 4b-d). The I κ B kinase
221 complex was also detected as being significantly activated. Activation of representative kinases of the
222 CMGC (ERK1&2) and the AGC (AKT1&2) groups was validated by an immunoblotting approach
223 (Supplementary Fig. 4a,b). To disentangle downstream effects of digoxin-mediated signalosome
224 activation, a genome-wide transcriptomic analysis was performed in similar conditions. As reported
225 in other systems²⁸, digoxin increased the expression of immediate-early genes (IEGs) such as *EGR-1*,
226 *c-FOS* and *c-JUN* both at low and high concentrations (Fig. 4e and Supplementary Dataset 3). Gene set
227 enrichment analysis of upregulated genes identified the NF κ B pathway as most robustly induced (Fig.

228 4f), in line with the phosphorylation of I κ B kinase subunits (Fig. 4b, c). Monitoring gene expression in
229 digoxin-exposed vs control mouse ZT9 hearts (Supplementary Dataset 4) showed an induction of *Egr-*
230 *1*, *c-Fos* and *c-jun* and other immediate early genes, with a 31% (12/38) overlap (Fig. 3e, see *) between
231 in vitro, digoxin-upregulated genes in AC16 cells and in vivo digoxin-upregulated genes in mouse heart.

232 Digoxin has been ascribed multiple effects owing to its ability to modulate the activity and/or
233 expression of several proteins: it modulates transcriptional activity of the nuclear receptor ROR γ ²⁹,
234 and interacts with PKM2 ³⁰, a target gene of HIF1 α whose translation is inhibited by digoxin ³¹.
235 Modulation of these pathways in AC16 cells by either a ROR γ inverse agonist (ML209, Supplementary
236 Fig. 5a), by knocking down *PKM2* (Supplementary Fig. 5b) or through *HIF1 α* overexpression
237 (Supplementary Fig. 5c) or activation (Supplementary Fig. 5d) did not blunt or exacerbate digoxin-
238 induced REV-ERB α degradation. Thus, these 3 established digoxin targets are not effectors of digoxin
239 action on REV-ERB α .

240 Thus, digoxin induces multiple signaling pathways, in murine cardiac tissue and cell lines,
241 without engaging previously identified CTS targets. The causal link between digoxin-mediated
242 induction of intracellular signaling pathways and altered REV-ERB α protein levels was further
243 investigated.

244

245 **The protein kinase SRC contributes to REV-ERB α stability.**

246 We first pharmacologically modulated the known digoxin-sensitive SRC tyrosine kinase and the
247 top-ranking digoxin-activated serine/threonine kinases identified above. We employed, in conjunction
248 or not with digoxin, widely-used chemical modulators for SRC (PP2), PI₃K (ZSTK474), ERK1&2
249 (SCH772984), AKTs (MK2206), CAMK1&2 (KN93), MEK1&2 (PD98059), PKG1&2 (RP8-pCPT-cGMPS),
250 PKD (CRT0066101), p70S6K1 (PF-4708671), RSK1&2&3 (BRD7389) and for components of the NF κ B
251 pathway such as LUBAC (Bay11-7082), HOIP (HOIPIN-8), IKK α / β (BMS345541), IKK β (TCPA-1), IKK ϵ and
252 TBK1 (amlexanox) (Fig. 5 and Extended data Fig. 5). This approach proved highly efficient at inhibiting
253 kinase activity (see Supplementary Fig. 4c as an example). Results were subsequently validated for a
254 number of targets using either overexpressed constitutively active kinase mutants, other inhibitors or
255 siRNAs (Extended data Fig. 6,7).

256 Stabilizing effects on basal REV-ERB α levels were observed when inhibiting PI3K, ERKs or MEKs
257 (Fig. 5). However, this was not confirmed using distinct inhibitors or siRNAs with the exception of PI3K
258 (Extended data Fig. 6). The latter effect was however not detected in U2OS cells (Supplementary Fig.

259 **6a**). Taken together, these data show that functional interference with this set of kinases did not
260 significantly affect REV-ERB α stability in basal conditions.

261 Blunting ERKs, PI3K, AKTs, CAMKs, MEKs, PKGs, PKD1, P70S6K1, RSKs, IKKs or TBK activity did
262 not impair digoxin's ability to trigger REV-ERB α degradation, a conclusion validated through the use of
263 alternative approaches (**Extended data Fig. 6,7**). In contrast, inhibition of SRC (with PP2, **Fig. 5a** and
264 with saracatinib, **Extended data Fig. 6a, 7a**) blunted digoxin-induced REV-ERB α protein decrease, an
265 effect which, albeit less pronounced, was also observed in U2OS cells (**Supplementary Fig. 6a**). This
266 data nevertheless suggested the involvement of SRC in the chain of events leading to decreased REV-
267 ERB α levels.

268 Bay 11-7082 efficiently stabilized REV-ERB α in non-challenged cells and significantly protected
269 REV-ERB α from digoxin-induced decreased expression in AC16 (**Fig. 5j and Extended data Fig. 5j**) and
270 U2OS cells (**Supplementary Fig. 13b**). Initially described as a linear ubiquitin chain assembly complex
271 (LUBAC) inhibitor, this compound also significantly inhibit several E2 ligases and the proteasome³².
272 The use of a more specific inhibitor of the LUBAC complex, HOIPIN-8³³ (**Fig. 5k and Extended data Fig.**
273 **5k**), of a *HOIL*-targeting siRNA (**Extended data Fig. 6j, 7j**) and the overexpression of the OUT domain-
274 containing deubiquitinase with linear linkage specificity (OTULIN, **Extended data Fig. 6k, 7k**) show no
275 significant effects in our assay, thereby excluding the LUBAC complex as contributing to the REV-ERB α
276 degradation process.

277 Since the NF κ B pathway was activated upon digoxin treatment, we assessed the involvement
278 of this transcription factor in several ways. We first **searched for** a transcriptomic blueprint of the
279 activated NF κ B pathway in cardiac tissues from *Nr1d1*^{-/-} mice. A comparative analysis of *Nr1d1*^{-/-} vs
280 *Nr1d1*^{+/+} heart transcriptome at ZT12 evidenced, alike the ZT0 vs ZT12 comparison (**Fig. 1b,c**), strong
281 dysregulation of clock-related processes without any significant enrichment in NF κ B-driven responses
282 (**Supplementary Fig. 7a**). Up- and downregulated genes were searched against the EnrichR ChEA
283 database to identify transcription factors binding in the vicinity of their promoters, on the basis of
284 aggregated CHIP-seq studies³⁴. This analysis did not identify NF κ B as a potential regulator of
285 dysregulated genes (**Supplementary Fig. 7b**). Overexpressing inhibitory wild type or super repressor
286 (SR) I κ B α ³⁵ did not protect or enhance digoxin's effect on REV-ERB α stability (**Supplementary Fig. 7c**).
287 Finally, the pharmacological NF κ B modulator betulinic acid did not prevent the effect of digoxin on
288 REV-ERB α protein levels, definitively excluding this pathway as a player in the observed REV-ERB α
289 degradation (**Supplementary Fig. 7d**).

290 Our results thus show that SRC kinase, described as part of the digoxin-controlled "NKA
291 signalosome", contributes to the observed decrease in REV-ERB α protein levels in AC16 and U2OS cells.

292 Bay 11-7082, which inhibits I κ B α , E2 ligases Ubc13 and UbcH7, the E3 ligase LUBAC and the
293 proteasome exerts a potent activity in our system, the effect of which being unrelated to the inhibition
294 of linear ubiquitylation by the LUBAC complex. These results rather pointed to the involvement of
295 UPS in REV-ERB α degradation.

296

297 **Digoxin induces the proteasomal degradation of REV-ERB α .**

298 The UPS and autophagy are 2 main branches of the protein quality control pathway.
299 Preliminary investigations ruled out other branches involving protein neddylation (using the NEDD8
300 inhibitor MLN4924/pevonedistat) or sumoylation (using the SUMO inhibitor 2-D08) as controlling REV-
301 ERB α stability (Supplementary Fig. 8). The autophagy pathway was not modulated by digoxin
302 (Supplementary Fig. 9a), contrasting with reports in cancerous cells 28557³⁶. Accordingly,
303 pharmacological modulation of autophagy by either chloroquine, bafilomycin or rapamycin did not
304 impact digoxin-induced effects (Supplementary Fig. 9b-d). Knocking down *P62/SQSTM1* expression,
305 which was the sole component of the autophagy pathway upregulated by digoxin (Supplementary Fig.
306 9a), had no effect (Supplementary Fig. 9e).

307 We then explored if the UPS is implicated in digoxin-induced REV-ERB α degradation. The
308 proteasome catalytic subunit beta 5 (PSBM5) inhibitors bortezomib (BTZ) and clasto-lactacystin β -
309 lactone, albeit to a lesser extent, protected REV-ERB α from digoxin-induced degradation (Fig. 6a,b and
310 Extended data Fig. 8a,b). Protection by BTZ was also observed in U2OS cells (Extended data Fig. 8c),
311 suggesting that UPS is a conserved component of the REV-ERB α degradation pathway. As
312 exogenously-expressed wild type REV-ERB α is equally sensitive to digoxin treatment (Fig. 6d and
313 Extended data Fig. 8d), we assessed whether REV-ERB α undergoes ubiquitylation and is modified
314 upon digoxin treatment using overexpressed Flag-REV-ERB α in AC16 cells. Mono-, multi- and poly-
315 ubiquitylated proteins were isolated from whole cell extracts and REV-ERB α content was analyzed
316 by western blot analysis. REV-ERB α was eluted along with other mono- and poly-ubiquitylated
317 proteins, and its concentration decreased in digoxin-exposed cellular extracts, and increased in
318 BTZ+digoxin-treated cells (Fig. 6e), indicative of a digoxin-controlled REV-ERB α ubiquitylation. The
319 H602F REV-ERB α mutant, which is unable to bind its natural ligand heme³⁷, showed higher expression
320 in basal conditions as reported³⁸ and was digoxin-resistant (Fig. 6d and Extended data Fig. 8d),
321 suggesting that heme binding to REV-ERB α promotes a conformation required for proteasomal
322 degradation.

323 To determine which component(s) of the UPS pathway could be involved in REV-ERB α
324 degradation, we isolated REV-ERB α interacting partners by RIME (rapid immunoprecipitation followed

325 by mass spectrometry identification of endogenous proteins)³⁹ using the digoxin-sensitive U2OS and
326 HepG2 cells. We then filtered the generated list of interactors against the Gene Ontology “cellular
327 component” or “molecular functions” databases using “proteasome” or “ubiquitin” as biological terms
328 and interacting significantly with REV-ERB α (Supplementary Dataset 6). We identified 16 UPS-related
329 proteins interacting with REV-ERB α , including several E2 (UBE2L3) and E3 (PRPF19, TRIM21) ubiquitin
330 ligases, the NCoR complex component TBL1XR1, and 4 subunits of the proteasome (PSMA4, PSMA5,
331 PSME3, PSMD2) (Fig. 7a). To this list of proteins potentially funneling REV-ERB α towards proteasomal
332 degradation, we added a number of E2 and E3/E4 ubiquitin ligases previously reported to regulate
333 REV-ERB α protein stability (SIAH2⁴⁰, FBWX7⁴¹, HUWE1⁴²) or predicted to act on REV-ERB α using the
334 proteome-wide E3 ligases-substrate interaction network (UbiBrowser⁴³) such as BRCA1, CBL, MDM2,
335 STUB1, TRIM33 and the ubiquitination factors UBE4A and UBE4B. The final list totaled 28 proteins (Fig.
336 7b), from which 19 were tested for their involvement in REV-ERB α degradation. AC16 cells were thus
337 transfected with siRNAs or treated with pharmacological inhibitors when available. Results are
338 summarized (Fig. 7) from the quantification (Extended data Fig. 9) of raw data (Extended data Fig. 10).
339 NEDD8, PSME3, the FBXW7-dependent destabilizing kinase CDK1⁴¹, the REV-ERB α stabilizing kinase
340 GSK3 β ⁴⁴, BRCA1, UBE4A, MDM2, STUB1 and TRIM33 were inactive in our assay (Extended data Fig. 9).
341 Six entities significantly contributed to REV-ERB α stability in basal conditions including the REV-ERB α -
342 interacting, NCoR complex component TBL1XR1 and the E3 ligases SIAH2, HUWE1, FBXW7, CBL and
343 UBE4B. Quite unexpectedly, impaired expression of the E2 ligase-encoding gene *UBE2L3/UBCH7*
344 decreased basal REV-ERB α expression (Extended data Fig. 9d). However, none of these E3 ligases
345 modulated the digoxin-mediated REV-ERB α degradation, with the exception of SIAH2, whose
346 knockdown partially maintained REV-ERB α level (Extended data Fig. 9a). Thus, digoxin-mediated
347 activation of UPS triggers REV-ERB α degradation through a complex chain of events yet to be
348 identified, but including the E3 ligase SIAH2 and the proteasome subunit PSMB5 (Fig. 8).

349

DISCUSSION

350

351 In the current era of precision medicine wherein therapies are formulated and administered
352 to attain maximal benefit through increased efficiency and reduced side effects, chronotherapy is an
353 important step further towards this goal. As an edifying example, chrono-chemotherapy is beneficial
354 in combating cancer by using a circadian window of higher drug tolerability and efficiency ⁴⁵.
355 Chronotherapy has been recently extended to hypertension treatment at bedtime, and proved more
356 efficient at decreasing CVD events ⁴⁶.

357 The unevenly distributed rate of occurrence of cardiac events suggest a differential sensitivity
358 of the heart to injury along the 24h day-night period ⁸. ToD dependent functional variations occur in
359 heart physiology, which are partly reflected by the significantly oscillating expression of approximately
360 13% of cardiac genes, which are involved in multiple functions from signaling and growth to
361 transcription and cardiac remodeling ^{3,47}. Similarly, proteomic analysis established striking differences
362 in night versus day protein levels in heart ⁴⁸, suggesting that timed cardiac proteostasis is crucial to
363 proper heart function. Along these lines, we reported a strong correlation between the time of surgery
364 and perioperative myocardial tolerance to injury in patients undergoing aortic valve replacement. This
365 ToD-dependent differential myocardial sensitivity to IRI was attributed to the rhythmic expression of
366 the nuclear receptor REV-ERB α and of its anti-apoptotic target gene *P21* ¹⁰. We also suggested the
367 therapeutic potential of pharmacological inhibition of REV-ERB α for prophylactic cardioprotection.
368 This provided an alternative approach to physical ischemic PC in which multiple distal, brief ischemic
369 episodes induce cardioprotective signaling pathways that bestow protection in a future event of
370 prolonged ischemia.

371 With the realization that NKA, the primary target of digoxin and other CTS, controls the
372 activation of multiple signaling pathways including part of the RISK and SAFE pathways such as AKT,
373 PKC and tyrosine kinases (Fig. 4), the use of CTS as PC agents has been proposed ¹⁶. Cardioprotection
374 is observed in rats dosed with a sub-ionic dose of ouabain followed by washout similarly to IPC
375 ^{25,49}. However, this strategy has not yet gained momentum, as digoxin use in heart failure and atrial
376 fibrillation has stirred a 200-year long history of controversies, leading to clinical hesitancy to widen
377 digoxin and other CTS use in PC and other pathologies ⁵⁰⁻⁵².

378 Our study however demonstrates a ToD-dependent action of digoxin on myocardial integrity.
379 The decreased susceptibility to IRI in mice dosed with digoxin when REV-ERB α expression reaches its
380 maximum (ZT9) could be potentially attributed to 2 principal effects: (1) circadian rhythm alteration
381 and/or (2) pharmacological cardiac preconditioning through the rapid and potent activation of many
382 components of the RISK and SAFE pathway including PI3K, AKT, ERK1/2, GSK3 β , and NF κ B (Fig. 3).

383 Genetic ablation of REV-ERB α showed that its expression is mandatory to observe digoxin protective
384 effects. Digoxin treatment in mice relieved REV-ERB α repression on several genes including the
385 cardioprotective *Bmal1* and *cdkn1a* (Extended data Fig. 1 and Supplementary Dataset 4). The anti-
386 apoptotic P21 is not required for the cardioprotective effect of digoxin. Cardioprotective activities of
387 BMAL1 have been elegantly documented through the use of genetic models⁵³. The ZT12-digoxin
388 phenotype is reminiscent of that of CCM mice, whose clock is locked at the wake-to-sleep transition
389 (ZT0), display improved tolerance to MIRI at ZT12 and in which *Bmal1* is similarly upregulated with
390 dampened cyclicality⁸. Identified BMAL1 target genes include *Nampt* or *Coq10b* which replenish cellular
391 stores in cardioprotective NAD⁺ and ubiquinone respectively⁵⁴. However, digoxin-exposed hearts
392 displayed no altered expression of these and other BMAL1 target genes (Supplementary Dataset 4), an
393 outcome likely due to the short time frame (4 hours) of the acute digoxin treatment. Thus, BMAL1 is
394 unlikely to play a role in the observed phenomenon.

395 In contrast to these cardioprotective effects at ZT9, digoxin treatment of REV-ERB α -depleted
396 hearts (ZT0) resulted in, albeit non-significant, trend to increased susceptibility to MIRI. As our
397 transcriptomic studies did not point to obvious mechanisms, the molecular basis for this differential
398 sensitivity to digoxin at ZT0 is unclear at this stage. Multiple parameters not assessable by gene
399 expression studies may indeed control heart sensitivity to MIRI. Circadian variations of heart
400 metabolism and temporal gating of signaling pathways may contribute to this time-specific response
401⁵³, while NKA α 1 expression is constant throughout the day-night cycle (Extended data Fig. 2 and⁵⁵).
402 Alternatively, the subcellular localization of NKA subunits, which is exquisitely regulated and
403 dependent on protein-protein interactions, may vary and affect its signaling properties.

404 An unexpected, yet one of the most important findings in our study is the impact of digoxin on
405 REV-ERB α protein levels in vivo and in human primary and immortalized cardiomyocytes. Exogenously
406 overexpressed REV-ERB α was found to be equally sensitive to digoxin and a target for the
407 ubiquitination machinery. In contrast, the overexpressed ligand binding-crippled H602F REV-ERB α
408 mutant was resistant to digoxin-induced degradation. Thus, heme-binding to REV-ERB α , which may
409 induce specific conformational changes in the aporeceptor structure, seems to be an important
410 prerequisite for physiological^(56,57 and Fig. 6d) and digoxin-triggered degradation through the
411 proteasomal pathway. Interestingly, heme regulatory motif (HRM)- or PAS (PER-ARNT-Sim)-containing
412 transcription factors and clock components such as NPAS2, CLOCK, PER1 and PER2 are also subjected
413 to heme-dependent protein degradation^{58,59,60}, linking heme synthesis and circadian rhythm
414 regulation.

415 Our data thus clearly point to a beneficial effect of acute REV-ERB α antagonism in
416 cardioprotection. This observation seems at odds with investigations reporting improvement of failing
417 hearts 1-day post-MI following treatment with SR9009, a REV-ERB agonist ⁶¹, which induces cardiac
418 transcriptomic alterations ^{62,63}, and blockade of cardiac remodeling through an anti-inflammatory
419 mechanism ⁶⁴. However, prolonged agonist treatment decreases, through a negative auto-feedback
420 loop, REV-ERB α protein level ⁶¹. Alternatively, it also triggers systemic immune cell mobilization ⁶⁵, a
421 process unlikely to be at play in our acute system.

422 CTS-controlled protein degradation is not unprecedented. Ouabain and digoxin triggers the
423 degradation of the nuclear estrogen receptor ER α in primary and metastatic breast cancer cells,
424 providing an additional mechanism for the reported CTS cytotoxicity against cancer cells ⁶⁶. Bufalin,
425 which also induces REV-ERB α degradation (**Extended data Fig. 3f**), strongly impacts on p160 steroid
426 receptor coactivator SRC1 and SRC3 protein stability ⁶⁷. Knockdown experiments however ruled out a
427 contribution of SRC1 and 3 in our system (**Supplementary Fig. 10**). The pleotropic effects of CTS thus
428 call for a careful examination of their side-effects. However, their use in cardiac PC as a timed, single,
429 low dose administration is an appealing therapeutic strategy to improve patient outcome, as
430 unwanted effects of these FDA-approved drugs will be predictably limited. On the contrary, prolonged
431 exposure to CTS in either CVD or cancer therapy might impinge on the molecular clock in several organs
432 including the liver (**Supplementary Fig. 2**), inducing metabolic alterations with unpredictable
433 outcomes. Alternative approaches may be considered to target REV-ERB α for elimination. Combining
434 REV-ERB α ligands to an E3 recognition motif to generate a PROteolysis TArgeting Chimera (PROTAC)
435 may be an innovative strategy to lessen heart susceptibility to MIRI.

436

437

METHODS

438 **Reagents**

439 All information about reagents, chemicals, siRNAs, Taqman probes, antibodies, plasmids, transfection
440 reagents, kits and softwares are provided in the accompanying [Supplementary Information file](#).

441

442 **Animal Experimentation**

443 All experiments were approved by the Comité d’Ethique en Expérimentation Animale du Nord-
444 Pas de Calais CEEA75. To eliminate sex as a confounder, male mice were used throughout this study.
445 C57BL6/J wild-type male mice (10-14 weeks) were purchased from Charles River Laboratories and
446 housed in a temperature-controlled environment (23-25°C, 40-60% humidity) with a 12h/12h light-
447 dark cycle, ZT0 being lights-on. Mice had free access to water and were fed ad libitum a standard chow
448 diet (Safe Diet A04). *Cdkn1a/p21*^{-/-} mice and their wild-type littermates were obtained from Charles
449 River (France, B6.129.S6(Cg)-Cdkn1atm1Led/J - SN 16565), *Nr1d1*^{-/-} mice (SV129.*Nr1d1*^{-/-68}) were bred,
450 housed and fed as above.

451 To study the impact of digoxin in vivo, animals were injected intraperitoneally with digoxin or
452 vehicle (10% ethanol, 40% propylene glycol, 0.08% citric acid, 0.3% sodium phosphate) at ZT5 or ZT20
453 at indicated concentrations (in most cases 1 mpk). The investigator was blinded to the treatment.
454 Mice were sacrificed by cervical dislocation at ZT9 or ZT0. Organs were harvested and snap-frozen for
455 protein and RNA analysis. Heart sensitivity to MIRI was tested using the ex vivo Langendorff perfused
456 mouse heart model⁶⁹. Isolated hearts were retrogradely perfused with a 5% CO₂-95% O₂-saturated
457 modified Krebs–Henseleit (118.5 mM NaCl, 25 mM NaHCO₃, 4.7 mM KCl, 1.2 mM MgSO₄, 1.2 mM
458 KH₂PO₄) buffer (1.4 mM Ca⁺⁺; 11 mM glucose) at a constant flow rate of 2.5 mL/min (Masterflex L/S
459 peristaltic pump) at 37°C with an imposed pacing (9 Hz, 540 bpm). Hearts were stabilized for 20 min
460 in these conditions then subjected to a normothermic, 30 min global ischemia by switching off the
461 coronary perfusion. Hearts were then re-perfused for 30 min. Heart linear contractions were
462 measured by passing a hook through the heart apex with a pre-load of 1.5 g and recorded. Perfusion
463 pressure was recorded with a Labtrax 4/24T (World Precision Instruments) device and integrated using
464 the LabScribe data acquisition and analysis software (v 2.0). Ex vivo preconditioning was achieved by
465 submitting hearts to an iterative (4 times) ischemia-reperfusion sequence (2x 5 min)(see [Fig. 1a](#)).

466 Infarct sizes were measured using the 2,3,5-triphenyltetrazolium chloride (TTC) staining
467 method. TTC (1%) was injected through the aortic canulae and incubated for 10 min at 37°C. Infarcted
468 (white) and viable (red) areas were measured by computerized planimetry (Adobe Photoshop).
469 Exclusion criteria for perfused hearts were a time to perfusion >3 min, a coronary perfusion pressure
470 > 140 mm Hg or < 40 mm Hg or raising transiently above 180 mm Hg.

471

472 ***Cell lines and human primary ventricular cardiomyocytes***

473 The AC16 human cardiomyocyte cell line ²¹ was from Millipore (SCC109). Cells were
474 maintained in DMEM/F12 Ham (Sigma-Aldrich) supplemented with 2mM L-glutamine (Thermo Fisher
475 Scientific), 12.5% of fetal bovine serum (FBS) and 1% penicillin-streptomycin (Thermo Fisher Scientific).

476 The U2OS cell line was from ATCC (HTB-96) and maintained in McCoy 5A medium (Thermo
477 Fisher Scientific) supplemented with 10% FBS and 1% penicillin–streptomycin.

478 Authenticated (STR-profiled) HepG2 cells were from ATCC (HB-8095) and grown in DMEM
479 containing 25 mM Glc supplemented with 10% FBS, 1 mM nonessential amino acids, 1 mM sodium
480 pyruvate, and 1% penicillin/streptomycin.

481 Human primary ventricular cardiomyocytes were from PromoCell (C-12811). These cells are
482 from ventricles of an explanted heart of a male donor who underwent heart transplantation. Cells
483 were tested and validated for cell specific markers, morphology, viability and adherence rate. Cells
484 were maintained in Myocyte Growth Medium (C-22070, PromoCell) supplemented with Myocyte
485 growth medium supplement mix (C-39270, PromoCell).

486 For all experiments, confluent cells were synchronized using 100nM dexamethasone (Sigma)
487 for 2 hours, then washed in 1x PBS. This defined T₀, after which cells were maintained in their
488 respective growth media for further experimentation. Cell sampling and treatment were performed
489 at indicated times. Cell viability was determined at indicated concentrations (see Fig. legends) using
490 CellTiter-Glo[®] Luminescent Cell Viability Assay (Promega, G7570). DMSO was used at concentrations
491 below 0.02% to avoid unwanted effects on REV-ERB α protein stability. Luciferase real-time recording
492 was as described ³³, with a stabilization period (T₀-T₁₂).

493 All cell lines were routinely (once a month) monitored for mycoplasma.

494

495 ***RNA extraction and RT-qPCR analysis***

496 RNA extraction from cultured cells was carried out using the NucleoSpin[®] RNA Midi kit
497 (Macherey-Nagel). Total RNA from mouse heart was extracted from samples pulverized in liquid
498 nitrogen using TRIzol[™] Reagent (Thermo Fisher Scientific). Prior to cDNA preparation with the High
499 Capacity cDNA Reverse Transcription kit (Thermo Fisher Scientific), total RNA extracts were subjected
500 to DNase I treatment. cDNAs were quantified using TaqMan Gene Expression Assays. Gene expression
501 was normalized to 18S rRNA expression and relative gene expressions were calculated using the 2^{- $\Delta\Delta$ Ct}
502 method ⁷⁰.

503

504 ***Protein extraction, Western blotting (WB) and Simple Western immunoassays***

505 Proteins were extracted using M-PER cell lysis buffer (Pierce) supplemented with Halt Protein
506 Phosphatase and Protease cocktail (1:100 dilution, Pierce). Following a brief vortexing and
507 centrifugation (30 min., 16,000 G), the supernatant protein concentration was determined using the
508 BCA protein assay kit (Pierce).

509 Protein expression level was studied either by western blotting or by WES Simple Western analysis
510 (Simple Western™)⁷¹.

511 • Western blotting: 20µg of protein were resolved by 12% SDS-PAGE under reducing conditions
512 and blotted onto a nitrocellulose membrane. The membrane was blocked in 5% BSA in 1x
513 TRIS-buffered Saline-Tween (TBS-T) and incubated overnight with the indicated antibody.
514 Membranes were washed 3 times in 1x TBS-T and incubated with an anti-mouse HRP-labelled
515 secondary antibody (1:10,000) for 1 hour. SuperSignal™ West Dura Extended Duration
516 substrate (Thermo Fisher Scientific) was used to detect antigen-antibody complexes.

517 • WES analysis: 3.8 µg proteins were resolved by size by capillary electrophoresis. After
518 immobilization onto the capillary by photoactivated capture chemistry, target proteins were
519 identified using specific primary antibodies (see Supplemental Information for references) and
520 immunoprobed using an HRP-conjugated secondary antibody and a chemiluminescent
521 substrate (ProteinSimple). Chemiluminescent signals were detected and quantified using the
522 Compass for SW software (ProteinSimple).

523 Protein levels were normalized to relative changes in HSP90AA1, β-actin or vinculin as indicated,
524 which were run in parallel on different gels/WES plates at the same time using the same biological
525 samples.

526

527 ***Cloning and transfection***

528 Transfections were performed 24 hours (T₋₂₄) prior to dexamethasone-induced
529 synchronization. The pEZ-M11-hREV-ERBα (plasmid Genecopoeia) (referred to as Flag-REV-ERBα) was
530 used to overexpress flagged human REV-ERBα or its derivatives. Human flagged REV-ERBα mutant
531 (hREV-ERBα-H602F) deficient in binding heme was generated using the Flag-REV-ERBα plasmid by
532 substituting H602 with F⁷².

533 The human *Bmal1*-luciferase construct (Bmal-Luc) used for real-time bioluminescence studies
534 was obtained by cloning the *Bmal1* promoter region (-350 to + 100) relative to the gene transcriptional
535 start site into the SV40-driven, red-emitting luciferase pCBR reporter vector (Promega).
536 Overexpression of wild type and constitutively active HIF1α was achieved by using HA-HIF1α-pcDNA3
537 (WT-HIF1α) and HA-HIF1α P402A/P564A-pcDNA3 (CA-HIF1α), respectively⁷³. These plasmids were
538 provided by W. Kaelin (Addgene plasmid # 18949, RRID: Addgene #18955Fugene HD® (Promega) was
539 used to transfect AC16 cells. Transfection of U2OS was achieved using JetPEI® (Polyplus Transfection).

540 For immunoprecipitation experiments, 10 μ g pEZ-M11-REV-ERB α were transfected into 1.1x10⁷ AC16
541 or U2OS cells. Transfection efficiency was controlled by RT-qPCR, western blotting or WES analysis.

542

543 ***Small interfering RNA***

544 Transfections were performed 24 hours (T₋₂₄) prior to dexamethasone-induced
545 synchronization. AC16 cells were transfected for 24 hours with 10nM siRNAs (Control: On-target plus
546 non-targeting pool or On-target plus Smart pool siRNAs; see details in the Appendix) using
547 Lipofectamine RNAiMAX (Thermo Fisher Scientific). Silencing experiments in U2OS cells were carried
548 out by transfecting 10nM siRNAs using INTERFERin[®] (Polyplus Transfection). Silencing efficiency was
549 monitored by RT-qPCR or western blotting.

550

551 ***Immunoprecipitation and ubiquitination assay***

552 Using the Crosslink Magnetic IP/Co-IP kit (Pierce), immunoprecipitation was carried out as
553 described earlier³³. For ubiquitination assays, 1.7x10⁷ cells were transfected with 10 μ g pEZ-M11-REV-
554 ERB α plasmid. On the following day, cells were treated with 0.5 μ M digoxin (Sigma-Aldrich) with or
555 without 1 μ M clasto-lactacystin β -lactone (Sigma-Aldrich) or 10 μ M bortezomib (Sigma-Aldrich) for 24
556 hours. Ubiquitinated proteins were captured using the UBI-CAPTURE-Q[®] kit (ENZO Life Sciences).
557 Ubiquitinated proteins were resolved by 10% SDS-PAGE and were probed with anti-REV-ERB α
558 antibody (Cell Signaling Tech.) or the anti-mono/polyubiquitinated conjugates monoclonal antibody
559 FK2 (ENZO Life Sciences).

560

561 ***PamGene Kinase Array***

- 562
- 563 • **Sample preparation:** AC16 cells were plated in 12-well fibronectin-gelatin coated plates
564 (Sigma). Cells were synchronized using 100nM dexamethasone as described above. Twenty
565 hours later, cells were treated with 0.5 or 5 μ M digoxin. After 4 hours of incubation, cells were
566 washed twice with 250 μ L 1x PBS and lysed in 250 μ L M-PER cell lysis buffer (Pierce)
567 supplemented with Halt Protein Phosphatase and protease inhibitors (Pierce). Lysates were
568 vortexed for 30 seconds and centrifugated (30 min., 16,000 G, 4°C). Protein concentration was
569 determined with the BCA protein assay kit (Pierce).
 - 570 • **PamStation Kinomic analysis:** Kinomic profiling of lysates was performed using a
571 PamStation[®]12 (PamGene Intl) and Serine/Threonine Kinase (STK) PamChip[®] Arrays. Each STK
572 PamChip[®] Array contains 144 peptides: 4 positive control phosphorylated peptides and 140
573 consensus phospho-peptide sequences representing the Ser/Thr kinome. Briefly, PamChip
574 arrays were blocked with 2% BSA (1-30 cycles). After the initial blocking step, 2 μ g proteins
from cell lysates premixed with 4 μ l of 10x PK buffer (PamGene), 0.4 μ l of 4mM ATP, 0.4 μ l of

575 100x BSA, and 0.5 μ l anti-STK primary antibody adjusted to a total volume of 40 μ l in distilled
576 water were added to individual PamChip arrays. The mix was then pumped (30 cycles) through
577 the PamChip[®] then arrays were washed with 1x PBS/0.01% Tween buffer followed by injection
578 of 30 μ l of PamChip detection mix [0.4 μ l of FITC-labelled anti-STK antibody (1 μ g/ μ l in TRIS
579 buffer, PamGene), 3 μ l of 10x Ab buffer (PamGene) and 26.6 μ l H₂O] . Real-time fluorescence
580 signal was quantified by EVOLVE (PamGene).

581 • **Image and data analysis of kinomic profiles:** The BIONAVIGATOR software Suite (PamGene)
582 was used to analyze images and to (\log_2) transform signal intensities. The kinase upstream
583 analysis algorithm within the BIONAVIGATOR Software Suite was employed to identify
584 putatively active kinases. A final score is calculated by the software based on the scores
585 obtained for specificity and significance. Kinases are ranked based on the mean final score
586 (MFS). A heat map was plotted using MFS scores. To visualize kinase activity changes in
587 digoxin-treated versus untreated cells/tissue, kinase trees were generated using the KinHub
588 platform (<http://www.kinhub.org/kinmap/>).

589

590 ***Microarray analysis, term enrichment analysis and network analysis***

591 Gene expression from mouse hearts or AC16 cells was analyzed with Affymetrix GeneChip Hu
592 (or Mo)Gene 2.0 ST arrays after RNA amplification, sscDNA labeling and purification. RNA was
593 amplified using the GeneChip[™] WT PLUS Reagent Kit (Thermo Fisher Scientific), retrotranscribed to
594 sscDNA and labeled using GeneChip[™] WT Terminal Labeling Kit (Thermo Fisher Scientific), followed by
595 hybridization on the GeneChip Mouse or Human Gene 2.0 ST Array (Affymetrix). Raw data were
596 processed using GIANT (Galaxy-based interactive tools for Analysis of Transcriptomic data ⁷⁴. Using
597 the GSEA module, normalized data were converted toward a GSEA compatible format for further
598 analysis.

599

600 ***Real-time measurement of bioluminescence***

601 Real-time monitoring of bioluminescence was performed using a Kronos AB-2550
602 luminometer (ATTO). AC16 or U2OS cells (1.1×10^7) were plated on P150 cell culture plates. When
603 reaching 80% confluency, cells were transfected with the *Bmal*-Luc plasmid (10 μ g) using either Fugene
604 HD[®] (Promega) or JetPEI[®] (Polyplus Transfection) for AC16 or U2OS cells, respectively. Twenty-four
605 hours after transfection, cells were split into 35mm cell culture dishes. Cells were synchronized
606 (100nM dexamethasone, 2 hours) and the medium was replaced with AC16 or U2OS phenol red-free
607 growth media. Cells were treated as indicated (see Fig. legends). Prior to starting light emission
608 monitoring, 200 μ M beetle luciferin (Promega) was added to growth medium. Bioluminescence was

609 measured for 1 min. at intervals of 10 min. under 5% CO₂ at 37°C for 4 days. Signals were quantified,
610 analyzed and detrended using the ATTO KRONOS software.

611

612 ***Rapid immunoprecipitation and mass spectrometry of endogenous proteins (RIME)***

613 RIME assays were performed using U2OS overexpressing Flagged-hREV-ERB α or HepG2 cells.
614 To overexpress REV-ERB α , cells were transfected with the Flag-REV-ERB α expression vector using
615 JetPEI (Polyplus transfection). Twenty-four hours after transfection, the medium was replaced by fresh
616 medium and cells were further incubated for 24h. Cells were synchronized (2h, 100 nM
617 dexamethasone), washed with 1x PBS and incubated for 20h with fresh media. Cells were cross-linked
618 for 10 min with 1% formaldehyde at 37°C in 1x DMEM. After quenching with 1.25 M glycine, cells were
619 washed twice with ice-cold 1x PBS. Fixed cells were scraped in ice-cold 1x PBS supplemented with
620 protease and phosphatase inhibitors (PIC, Roche). After centrifugation (1,000g, 10 min, 4°C), cells were
621 lysed in 50 mM HEPES-KOH pH 7.5, 140 mM NaCl, 1 mM EDTA, 10% glycerol, 0.5% NP40, 0.25% Triton
622 X-100 buffer supplemented with PIC. After centrifugation (1,000g, 10 min, 4°C), supernatants
623 (cytosolic fraction) and pellets (nuclear fraction) were collected. Pellets were washed in 10 mM TRIS-
624 HCl pH8.0, 200 mM NaCl, 1 mM EDTA and 0.5 mM EGTA buffer containing PIC, then in 10 mM TRIS-
625 HCl pH8.0, 200 mM NaCl, 1 mM EDTA and 0.5 mM EGTA, 0.1% sodium deoxycholate and 0.5% N-
626 laurylsarcosine buffer (with PIC). Nuclei were suspended into 50 mM HEPES-KOH pH 7.5, 1 mM EDTA,
627 0.5 M LiCl₂, 0.7% sodium deoxycholate, 1% NP40 and 1x PIC. After a 10 min sonication, Triton X-100
628 (1% v:v final) was added and samples were centrifuged at 20,000g for 10 min, yielding the nuclear
629 extract. In parallel, SureBeadsTM Protein A or G magnetic beads (Bio-Rad) were saturated with 5 mg/mL
630 BSA. Four μ g of rabbit monoclonal anti-REV-ERB α antibody (#13418, Cell Signalling Technology), 10 μ g
631 of mouse monoclonal anti-Flag antibody (#F1804, Sigma-Aldrich), 10 μ g of control rabbit IgG (sc-2027,
632 Santa Cruz Biotechnology) or mouse IgG (sc-2025, Santa Cruz Biotechnology) were immobilized on
633 SureBeadsTM Protein A (Rabbit) or G (Mouse) magnetic beads.

634 After centrifugation, cytosolic or nuclear extracts were incubated overnight with immobilized
635 antibodies at 4°C. Beads were washed with 1x RIPA buffer [50 mM HEPES-KOH, pH 7.6, 1 mM EDTA,
636 0.7% (v:v) sodium deoxycholate, 1% (v:v) NP-40 and 0.5 M LiCl] then with 0.1 M ammonium hydrogen
637 carbonate. Beads were dried and flash-frozen in liquid nitrogen. LC-MS/MS analysis was performed to
638 identify REV-ERB α interactants as described ⁷².

639

640 ***Apoptosis and autophagy antibody arrays***

641 To evaluate global changes in the apoptosis and autophagic pathways in digoxin-treated cells,
642 the Human Apoptosis Array C1 (AAH-APO-1-2, Raybiotech) and the Autophagy Array C1 (AAH-ATG-1-
643 2, Raybiotech) were employed. These arrays detect 43 and 20 human proteins regulating apoptosis
644 and autophagy, respectively. Briefly, AC16 cells were plated in P150 cell culture plates. At confluence,
645 cells were synchronized as above. Eighteen hours post synchronization, cells were treated either with
646 0.5 μ M digoxin or vehicle and lysed 6h later (T₂₄) in lysis buffer (Raybiotech). Antibody arrays were
647 blocked using the blocking buffer (2 mL, Raybiotech) for 30 minutes and 250 μ g of fresh total protein
648 lysate (1 mL) was added to each antibody array (1 sample/array). Arrays were incubated overnight at
649 4°C, then washed thoroughly in washing buffer (1 mL/wash, Raybiotech) and were further incubated
650 overnight at 4°C with biotinylated antibody cocktail (1 mL, Raybiotech). Arrays were washed twice (1
651 mL/wash) then incubated in 1x HRP-Streptavidin Concentrate for 2h at room temperature. All
652 blocking, washing and incubation steps were performed under gentle rotation (0.5-1 cycle/sec). After
653 a 2h incubation, arrays were washed once followed by chemiluminescence detection using an
654 Invitrogen™ iBright™ FL1500 Imaging System (Thermo Fisher Scientific). Spot intensities on each array
655 were quantified using Image Studio™ Lite (LI-COR Biosciences). The RayBiotech Microsoft® Excel-
656 based analysis software tool was used to average, normalize and subtract the background signal.
657 Heatmaps were generated using GraphPad Prism (v. 9.4).

658

659 ***Statistics and reproducibility***

660 Statistical analysis was performed using GraphPad Prism (v. 9.4). Data are plotted as the mean
661 \pm SEM. At least 3 independent experimental replicates were obtained. In vitro data were determined
662 to have equal variances using the F test. For 2-group comparisons, an unpaired 2-tailed *t*-test with
663 Welch correction was used. For multiple comparisons with one variable, a 1-way ANOVA followed by
664 the Tukey multiple comparison test (each group compared to every other group) was used. Multiple
665 comparisons with more than one variable were carried out using a 2-way ANOVA followed by a Tukey's
666 multiple comparison test. Cyclical patterns of gene expression or of protein levels were determined
667 using JTK_Cycle⁷⁵. Individual expression/level data were plotted in Prism as a time series and non-
668 linearly fitted using the "sine wave with nonzero baseline" function, using a wavelength constraint
669 previously determined by JTK_cycle (in the 20-24 hours range). For infarct size measurements, based
670 on an observed standard deviation of 8%, with α set at 0.05, β at 0.20 and a size effect of 10%, the
671 group size was set at n=7. In vivo datasets were considered to have unequal variances and groups
672 were compared using either a one-sided Welch's *t*-test, or a Welch ANOVA followed by the Dunnett
673 multiple comparison test unless mentioned otherwise. In all instances, P values < 0.05 were
674 considered statistically significant. All samples used in this study were biological replicates, not

675 technical replicates. All experiments were independently performed at least twice to reproduce similar
676 results.

677 Differential gene expression was analyzed after normalization of signals to the median of all
678 samples, \log_2 transformation and exclusion of the 10th lowest percentile considered as technically
679 unreliable. The Limma package, based on an Empirical Bayes method, is embedded into the Giant suite
680 and was used to identify genes exhibiting an expression fold-change > 1.2 with an FDR < 0.05
681 (moderated t-test followed by a Benjamini-Hochberg multiple testing correction). Biological term
682 enrichment analysis was performed using the DAVID NCBI portal (v6.8) ⁷⁶.

683

684 **Reporting summary**

685 Further information on research design is available in the Nature Research Reporting Summary
686 linked to this article.

687

688
689
690
691
692
693
694
695
696
697

Data availability

All data are available in the main text or the supplementary materials. Source data are available for this paper. Microarray data that support the finding of this study has been deposited in the National Center of Biotechnology Information's Gene Expression Omnibus and are accessible through accession number GSE183659, GSE183660 and GSE183661. Other transcriptomic datasets have been described in ¹⁰ and deposited under the accession number GSE62459. Whole mouse heart circadian gene expression was analyzed using the GSE180108 dataset ⁴⁷. The mass spectrometry proteomics data have been deposited to the ProteomeXchange Consortium via the PRIDE ⁷⁷ partner repository with the dataset identifier PXD03660

698

ACKNOWLEDGMENTS

699 We are grateful to Dr J. Vandel for help with transcriptomic data visualization, Prof S. Susen (CHRU
700 Lille, France) for generously providing DigiFab, and to Faris Najj (PamGene, Netherlands) for help and
701 advices for the PamGene data analysis. This work was supported by grants from INSERM (PL), Région
702 Hauts-de-France and Université de Lille (REV-ERBalpha/SAS20215, PL), from ANR [LABX EGID (ANR-10-
703 LABX-0046, BS); ANR VasCal (ANR46-CE14-0001-01, BS), ANR-CE14-0003-01 (DM), ANR-18-CE17-0003-
704 02 (DM); PreciDiab ANR-18-IBHU-0001; 20001891/NP0025517; 2019_ESR_11 (DM), ANR-17-CE14-
705 0034 (JSA), from the Leducq Foundation (LEAN network 16CVD01, BS), from Institut Pasteur de Lille
706 (CTRL Melodie, JSA), from the Fondation pour la Recherche Médicale (EQU202103012732, JSA). BS is
707 a recipient of an Advanced ERC Grant (694717)

708

709

AUTHOR'S CONTRIBUTIONS STATEMENT

710 Conceptualization: MV, PL, BS; Methodology: MV, JSA, AB, AH, SC, JE, PL; Validation: MV, CG, AH, SC,
711 AB, PL; Formal analysis: MV, PL; Investigation: MV, CG, XM, AB, AH, SC, RB; Resources: PL, BS, JE, HD,
712 SD, DM, JSA; Data visualization: MV, PL; Supervision: PL, BS; Funding acquisition: PL, BS.

713

714

COMPETING INTERESTS STATEMENT

715 Nothing to report

716

717

FIGURE LEGENDS

718 **Fig. 1. Time of the day- and REV-ERB α -dependent effects of digoxin in mouse heart. (a)** Time of the
719 day dependency of mouse heart sensitivity to MIRI and preconditioning (PC). Upper panel:
720 experimental outline. Lower panel: infarct sizes at ZT0 and ZT12, with or without prior exposure to an
721 iterative short ischemia/reperfusion sequence. Results are shown as mean \pm -SEM (n=8-9) which were
722 compared using a two-way ANOVA test, followed by a Benjamini-Hochberg multiple comparison test.
723 Infarct sizes were calculated based on necrosis area/area at risk. **(b)** Left panel: overrepresented Gene
724 Ontology Biological Processes (GO BP) terms in differentially expressed genes (ZT0 vs ZT12) mouse
725 hearts; right panel: up- or downregulated and/or rhythmically-expressed (period=22-24h) genes. **(c)**
726 Time-dependent expression of mouse heart genes. Normalized expression data are expressed as mean
727 \pm -SEM (n=3). **(d)** MIRI at ZT0 or ZT9 in wild type mouse hearts after injection of vehicle or digoxin (IP:
728 1mg/kg). **Top:** experimental outline and representative transversal sections of TTC-stained mouse
729 hearts post IR (red stain: healthy tissue, unstained: necrotic tissue); **Bottom:** infarct size
730 measurements. Results are shown as mean \pm -SEM (n=7-13) which were compared using two-way
731 ANOVA test, followed by a Benjamini-Hochberg multiple comparison test. **(e)** REV-ERB α protein level
732 in mouse heart whole extracts. Upper panel: representative Wes analysis of REV-ERB α protein levels
733 in mouse whole hearts. Bottom panel: quantification of REV-ERB α protein levels as a function of time.
734 Results are shown as mean \pm -SEM (n=3-4, see also Supplementary Fig. 2a) which were and compared
735 using Brown-Forsythe & Welch ANOVA test, followed by Dunnett's multiple comparison test. **(f)** In
736 vivo digoxin ED₅₀. REV-ERB α levels were assessed at ZT9 in whole heart extracts. Results are shown
737 as mean \pm -SEM (n=9-16, see also Supplementary Fig. 2b) which were analyzed using nonlinear fit
738 regression (least square method). **(g)** MIRI at ZT9. Myocardial IR tolerance was evaluated at ZT9 in
739 wild type vs *Nr1d1*^{-/-} or *Cdkn1a*^{-/-} mouse hearts treated either with vehicle or digoxin (ZT5, IP: 1mg/kg).
740 Results are shown as mean \pm -SEM (n=6-7) which were compared using a two-tailed Welch's t-test. All
741 measurements were from distinct samples.

742 **Fig. 2. Digoxin affects REV-ERB α protein stability in a cell-autonomous manner. (a)** Cyclic REV-
743 ERB α protein levels in AC16 cells. Top panel: experimental outline. REV-ERB α levels were determined
744 in synchronized human AC16 cells treated with vehicle or digoxin (0.5 μ M) at T₀ and harvested at T₀, T₆,
745 T₁₂, T₁₈ and T₂₄. Dex: dexamethasone. Bottom panel: Representative image from WES analysis.
746 HSP90 α was used as a protein loading control. Numbers indicate mean fold-changes [relative to
747 maximal REV-ERB α expression (24h, untreated cells)]. Results are shown as mean \pm -SEM (n=3) which
748 were compared using a one-way ANOVA test, followed by a Tukey's multiple comparison test (see
749 [Extended data Fig. 3a](#)). *: **: P<0.01, ***: P<0.005. **(b)** *NR1D1* and *BMAL1* mRNA expression in
750 synchronized AC16 cells. Cells were treated with vehicle or digoxin (0.5 μ M) at T₀ and harvested at T₂₄

751 (n=5). Results are shown as mean+/-SEM (n=5) which were compared using an unpaired two-sided t-
752 test. **(c)** Real-time monitoring of the *BMAL1* promoter activity. Top panel: experimental outline.
753 Bottom panel: bioluminescence signal measured using a KRONOS (Atto) luminometer in AC16 cells
754 transfected with the *Bmal1*-Luc(iferase) plasmid and treated with vehicle or digoxin (0.5 μ M) (n=3).
755 **(d)** CDKN1A/P21 protein level in AC16 cells. P21 level was assessed using the ProteinSimple Wes
756 system in AC16 cells treated with vehicle or digoxin (0.5 μ M). Results are shown as mean+/-SEM (n=5)
757 which were compared using a unpaired two-sided t-test. ***: P<0.005. HSP90 α was used as a protein
758 loading control. All measurements were from distinct samples.

759 **Fig. 3. Digoxin effect in human primary cardiomyocytes.** **(a)** Rhythmic REV-ERB α protein level.
760 Synchronized primary human cardiomyocyte cells were treated with vehicle or digoxin (0.5 μ M) and
761 harvested over a 36-hour period as indicated. **(b)** *NR1D1* and *BMAL1* mRNA expression in human
762 primary cardiomyocytes. Normalized data are plotted as mean+/-SEM (n=5) and compared using a
763 one-way ANOVA test, followed by a Tukey's multiple comparison test. Vinculin was used as a protein
764 loading control. All measurements were from distinct samples.

765 **Fig. 4. Intracellular pathways activation by digoxin.** **(a)** NKA ion pumping vs signalosome activities.
766 Top panel: experimental outline. Synchronized AC16 cells were treated as indicated for 6 hours at T18
767 and harvested at T₂₄. Dex: dexamethasone. Bottom panel: REV-ERB α protein levels in control and
768 treated cells. HSP90 α was used as a protein loading control. Right panel: normalized REV-
769 ERB α protein level. Results are shown as mean+/-SEM (n=10, see also Supplementary Fig. 7) which
770 were compared using a one-way ANOVA test, followed by a Tukey's multiple comparison test. **(b,c)**
771 Kinase activation trees in AC16 cells generated by KinMap using kinase profiling data at low **(b)** or high
772 **(c)** digoxin treatment concentration. Circle diameters are proportional to the level of activity of
773 kinases. **(d)** Heat map quantifying dose-dependent changes in kinase activities (n=3; 1-way ANOVA, *:
774 P<0.05). MFS: median final score. **(e)** Transcriptomic analysis in vehicle- or digoxin-treated (0.5 μ M,
775 5 μ M) AC16 cells. The heatmap shows the top-ranking 25 genes and indicates dose-dependent changes
776 in mRNA expression. Stars indicate genes whose expression is also altered in mouse heart after digoxin
777 treatment at ZT9. **(f)** Gene set enrichment analysis of upregulated genes in digoxin-treated AC16 cells.

778 **Fig. 5. Target screening with kinase specific and pathway specific inhibitors.** REV-ERB α protein levels
779 were quantified after a 6 hour-treatment (at T₁₈) with or without digoxin and with or without enzyme
780 inhibitors: **(a)** PP2 (20 μ M, Src kinase inhibitor), **(b)** ZSTK474 (10 μ M, PI3 kinase inhibitor), **(c)** SCH772984
781 (20 μ M, ERK 1&2 inhibitor), **(d)** MK2206 (1 μ M, AKT1/2/3 kinase inhibitor), **(e)** KN93 (1 μ M, CAMK 2&4
782 inhibitor), **(f)** PD98059 (20 μ M, MEK 1&2 inhibitor), **(g)** RP-8-pCPT-cGMPS (20 μ M, PKG1&2), **(h)**
783 CRT0066101 (5 μ M, PKD inhibitor), **(i)** PF-4708671 (10 μ M, P70S6K1 inhibitor), **(j)** BAY11-7082 (10 μ M,

784 LUBAC and UPS inhibitor), **(k)** HOIPIN8 (10 μ M, LUBAC-HOIP specific inhibitor), **(l)** BMS-345541 (10 μ M,
785 IKK α/β inhibitor), **(m)** TPCA-1 (20nM, IKK β **(n)** Amlexanox (20 μ M, IKK ϵ & TBK1 inhibitor). HSP90 α was
786 used as a protein loading control. Results are shown as mean \pm -SEM (n=3-6) which were compared
787 using a one-way ANOVA test, followed by a Tukey's multiple comparison test. All measurements were
788 from distinct samples.

789 **Fig. 6. Digoxin triggers REV-ERB α protein degradation through UPS.** REV-ERB α protein levels were
790 quantified after a 6 hour-treatment with or without digoxin and with or without the following
791 proteasome inhibitors in synchronized AC16 cells **(a)** clasto-lactacystin β -lactone (10 μ M, proteasomal
792 inhibitor), **(b)** bortezomib (BTZ, 200nM, PSMB5 inhibitor) and in synchronized U2OS cells **(c)** treated
793 with either vehicle, digoxin (0.5 μ M) and/or bortezomib (200nM, PSMB5 inhibitor). Results are shown
794 as mean \pm -SEM (n=3-6) which were compared using a one-way ANOVA test, followed by a Tukey's
795 multiple comparison test. **(d)** Normalized REV-ERB α protein level was assessed in synchronized AC16
796 cells transfected with Flag-Rev-ERB α or Flag-Rev-ERB α -H602F-encoding plasmids and treated with
797 vehicle or digoxin (0.5 μ M). HSP90 α was used as a protein loading control Results are shown as
798 mean \pm -SEM (n=5) which were compared using a one-way ANOVA test, followed by a Tukey's multiple
799 comparison test. **(e)** Western blot analysis of total ubiquitinated proteins and of ubiquitinated REV-
800 ERB α protein from cell lysates of U2OS cells transfected with Flag-Rev-ERB α plasmid and treated with
801 either vehicle, digoxin (0.5 μ M) and/or bortezomib (BTZ, 200nM, PSMB5 inhibitor) for 2 hours (T18 to
802 T20). Mono- and poly-ubiquitinated proteins in the lysate were enriched by passing it through a High
803 binding affinity UBI-QAPTURE-Q[®] matrix. All measurements were from distinct samples. *: P<0.05,
804 **: P<0.01, ***: P<0.001, ****: P<0.0001.

805 **Fig. 7. UPS-related REV-ERB α interactants.** **(a)** REV-ERB α interactants extracted from the RIME
806 dataset filtered against the Gene Ontology "cellular component" or "molecular functions" databases
807 using "proteasome" or "ubiquitin" as biological terms. Green lines indicate known direct interactions
808 as extracted from the String database. Red lines indicate detected direct or indirect interactions with
809 REV-ERB α by RIME. Distances between REV-ERB α and interactants are inversely proportional to the
810 number of identified peptides in the RIME data. Protein structures are from the AlphaFold Protein
811 Structure database. **(b)** Outcome of REV-ERB α interactant inhibition on digoxin-induced REV-ERB α
812 degradation. The table indicates the list of targets (identified from RIME and literature survey) studied
813 here using siRNA- and/or inhibitor-based strategies, and the outcome of such inhibition on REV-ERB α
814 protein level levels. Upward arrow: increased REV-ERB α protein level; downward arrow: decreased
815 REV-ERB α protein level; equal sign: no change.

816 **Fig. 8: Hypothetical scheme for digoxin action in cardiomyocytes.** The main pathways activated by
817 digoxin and the impact thereof on REV-ERB α protein stability are shown. More details can be found in
818 the text.

819

820

REFERENCES

821

- 822 1 Patke, A., Young, M. W. & Axelrod, S. Molecular mechanisms and physiological importance of
823 circadian rhythms. *Nat Rev Mol Cell Biol* **21**, 67-84 (2020).
- 824 2 Martino, T. A. & Young, M. E. Influence of the cardiomyocyte circadian clock on cardiac
825 physiology and pathophysiology. *J Biol Rhythms* **30**, 183-205 (2015).
- 826 3 Zhang, J., Chatham, J. C. & Young, M. E. Circadian Regulation of Cardiac Physiology: Rhythms
827 That Keep the Heart Beating. *Annu Rev Physiol* **82**, 79-101 (2020).
- 828 4 Crnko, S., Du Pre, B. C., Sluiter, J. P. G. & Van Laake, L. W. Circadian rhythms and the molecular
829 clock in cardiovascular biology and disease. *Nat Rev Cardiol* **16**, 437-447 (2019).
- 830 5 Hausenloy, D. J. & Yellon, D. M. Myocardial ischemia-reperfusion injury: a neglected
831 therapeutic target. *J Clin Invest* **123**, 92-100 (2013).
- 832 6 Hausenloy, D. J. & Yellon, D. M. Ischaemic conditioning and reperfusion injury. *Nat Rev Cardiol*
833 **13**, 193-209 (2016).
- 834 7 Rossello, X. & Yellon, D. M. The RISK pathway and beyond. *Basic Res Cardiol* **113**, 2 (2018).
- 835 8 Durgan, D. J. *et al.* Short communication: ischemia/reperfusion tolerance is time-of-day-
836 dependent: mediation by the cardiomyocyte circadian clock. *Circ Res* **106**, 546-550 (2010).
- 837 9 Janszky, I. L., R. Shifts to and from Daylight Saving Time and Incidence of Myocardial Infarction.
838 *N Engl J Med* **359**, 1966-1968 (2008).
- 839 10 Montaigne, D. *et al.* Daytime variation of perioperative myocardial injury in cardiac surgery
840 and its prevention by Rev-Erba antagonism: a single-centre propensity-matched cohort study
841 and a randomised study. *The Lancet* **391**(10115),59-69. (2018).
- 842 11 Davidson, S. M. *et al.* Multitarget Strategies to Reduce Myocardial Ischemia/Reperfusion
843 Injury: JACC Review Topic of the Week. *J Am Coll Cardiol* **73**, 89-99 (2019).
- 844 12 Fellahi, J. L., Fischer, M. O., Daccache, G., Gerard, J. L. & Hanouz, J. L. Positive Inotropic Agents
845 in Myocardial Ischemia–Reperfusion Injury. *Anesthesiology* **118**, 1460-1472 (2013).
- 846 13 Matsui, H. & Schwartz, A. Mechanism of cardiac glycoside inhibition of the (Na⁺-K⁺)-
847 dependent ATPase from cardiac tissue. *Biochim Biophys Acta* **151**, 655-663 (1968).
- 848 14 Askari, A. The sodium pump and digitalis drugs: Dogmas and fallacies. *Pharmacol Res Perspect*
849 **19**,7:e00505 (2019).
- 850 15 Liang, M. *et al.* Identification of a pool of non-pumping Na/K-ATPase. *J Biol Chem* **282**, 10585-
851 10593 (2007).
- 852 16 Marck, P. V. & Pierre, S. V. Na/K-ATPase Signaling and Cardiac Pre/Postconditioning with
853 Cardiotonic Steroids. *Int J Mol Sci* **19**,2336 (2018).

- 854 17 Nelson, W., Kupferberg, H. & Halberg, F. Dose-response evaluations of a circadian rhythmic
855 change in susceptibility of mice to ouabain. *Toxicol Appl Pharmacol* **18**, 335-339 (1971).
- 856 18 Patocka, J., Nepovimova, E., Wu, W. & Kuca, K. Digoxin: Pharmacology and toxicology-A review.
857 *Environ Toxicol Pharmacol* **79**, 103400 (2020).
- 858 19 Dostanic, I. *et al.* The alpha2 isoform of Na,K-ATPase mediates ouabain-induced cardiac
859 inotropy in mice. *J Biol Chem* **278**, 53026-53034 (2003).
- 860 20 Iisalo, E. Clinical pharmacokinetics of digoxin. *Clinical pharmacokinetics* **2**, 1-16 (1977).
- 861 21 Davidson, M. M. *et al.* Novel cell lines derived from adult human ventricular cardiomyocytes.
862 *J Mol Cell Cardiol* **39**, 133-147 (2005).
- 863 22 Felipe Gonçalves-de-Albuquerque, C., Ribeiro Silva, A., Ignácio da Silva, C., Caire Castro-Faria-
864 Neto, H. & Burth, P. Na/K Pump and Beyond: Na/K-ATPase as a Modulator of Apoptosis and
865 Autophagy. *Molecules* **22**, 578 (2017).
- 866 23 Balsalobre, A., Marcacci, L. & Schibler, U. Multiple signaling pathways elicit circadian gene
867 expression in cultured Rat-1 fibroblasts. *Curr Biol* **10**, 1291-1294 (2000).
- 868 24 Katz, A. *et al.* Selectivity of digitalis glycosides for isoforms of human Na,K-ATPase. *J Biol Chem*
869 **285**, 19582-19592 (2010).
- 870 25 Morgan, E. E. *et al.* Preconditioning by subinotropic doses of ouabain in the Langendorff
871 perfused rabbit heart. *Journal of cardiovascular pharmacology* **55**, 234-239 (2010).
- 872 26 Duan, Q. *et al.* Preconditioning and Postconditioning by Cardiac Glycosides in the Mouse Heart.
873 *Journal of cardiovascular pharmacology* **71**, 95-103 (2018).
- 874 27 Zhang, Z. *et al.* Identification of hydroxyxanthones as Na/K-ATPase ligands. *Mol Pharmacol* **77**,
875 961-967 (2010).
- 876 28 Orlov, S. N. *et al.* Na(+),K(+)i-Dependent and -Independent Signaling Triggered by Cardiotonic
877 Steroids: Facts and Artifacts. *Molecules* **22**, 635 (2017).
- 878 29 Huh, J. R. *et al.* Digoxin and its derivatives suppress TH17 cell differentiation by antagonizing
879 ROR γ activity. *Nature* **472** (2011).
- 880 30 Ouyang, X. *et al.* Digoxin Suppresses Pyruvate Kinase M2-Promoted HIF-1 α Transactivation
881 in Steatohepatitis. *Cell Metab* **27**, 339-350 (2018).
- 882 31 Zhang, H. *et al.* Digoxin and other cardiac glycosides inhibit HIF-1 α synthesis and block
883 tumor growth. *Proc Natl Acad Sci U S A* **105**, 19579-19586 (2008).
- 884 32 Strickson, S. *et al.* The anti-inflammatory drug BAY 11-7082 suppresses the MyD88-dependent
885 signalling network by targeting the ubiquitin system. *Biochem J* **451**, 427-437 (2013).
- 886 33 Oikawa, D. *et al.* Molecular bases for HOIPINs-mediated inhibition of LUBAC and innate
887 immune responses. *Commun Biol* **3**, 163 (2020).
- 888 34 Xie, Z. *et al.* Gene Set Knowledge Discovery with Enrichr. *Current protocols* **1**, e90 (2021).

889 35 Brown, K., Gerstberger, S., Carlson, L., Franzoso, G. & Siebenlist, U. Control of I kappa B-alpha
890 proteolysis by site-specific, signal-induced phosphorylation. *Science* **267**, 1485-1488 (1995).

891 36 Wang, Y. *et al.* Cardiac glycosides induce autophagy in human non-small cell lung cancer cells
892 through regulation of dual signaling pathways. *Int J Biochem Cell Biol* **44**, 1813-1824 (2012).

893 37 Raghuram, S. *et al.* Identification of heme as the ligand for the orphan nuclear receptors REV-
894 ERBalpha and REV-ERBbeta. *Nat Struct Mol Biol* **14**, 1207-1213 (2007).

895 38 Carter, E. L., Gupta, N. & Ragsdale, S. W. High Affinity Heme Binding to a Heme Regulatory
896 Motif on the Nuclear Receptor Rev-erbbeta Leads to Its Degradation and Indirectly Regulates
897 Its Interaction with Nuclear Receptor Corepressor. *J Biol Chem* **291**, 2196-2222 (2016).

898 39 Mohammed, H. *et al.* Rapid immunoprecipitation mass spectrometry of endogenous proteins
899 (RIME) for analysis of chromatin complexes. *Nat Protoc* **11**, 316-326 (2016).

900 40 DeBruyne, J. P., Baggs, J. E., Sato, T. K. & Hogenesch, J. B. Ubiquitin ligase Siah2 regulates
901 RevErbalpha degradation and the mammalian circadian clock. *Proc Natl Acad Sci U S A* **112**,
902 12420-12425 (2015).

903 41 Zhao, X. *et al.* Circadian Amplitude Regulation via FBXW7-Targeted REV-ERBalpha Degradation.
904 *Cell* **165**, 1644-1657 (2016).

905 42 Yin, L., Joshi, S., Wu, N., Tong, X. & Lazar, M. A. E3 ligases Arf-bp1 and Pam mediate lithium-
906 stimulated degradation of the circadian heme receptor Rev-erb alpha. *Proc. Natl. Acad. Sci. U.*
907 *S. A* **107**, 11614-11619 (2010).

908 43 Li, Y. *et al.* An integrated bioinformatics platform for investigating the human E3 ubiquitin
909 ligase-substrate interaction network. *Nat Commun* **8**, 347 (2017).

910 44 Yin, L., Wang, J., Klein, P. S. & Lazar, M. A. Nuclear receptor Rev-erba is a critical lithium-
911 sensitive component of the circadian clock. *Science* **311**, 1002-1005 (2006).

912 45 Hill, R. J. W., Innominato, P. F., Levi, F. & Ballesta, A. Optimizing circadian drug infusion
913 schedules towards personalized cancer chronotherapy. *PLoS Comput Biol* **16**, e1007218
914 (2020).

915 46 Hermida, R. C. *et al.* Bedtime hypertension treatment improves cardiovascular risk reduction:
916 the Hygia Chronotherapy Trial. *Eur Heart J* **41**, 4565-4576 (2020).

917 47 Martino, T. *et al.* Day/night rhythms in gene expression of the normal murine heart. *J Mol Med*
918 *(Berl)* **82**, 256-264 (2004).

919 48 Podobed, P. *et al.* The day/night proteome in the murine heart. *Am J Physiol Regul Integr Comp*
920 *Physiol* **307**, R121-137 (2014).

921 49 Duan, Q. *et al.* Role of phosphoinositide 3-kinase IA (PI3K-IA) activation in cardioprotection
922 induced by ouabain preconditioning. *J Mol Cell Cardiol* **80**, 114-125 (2015).

923 50 Digitalis Investigation, G. The effect of digoxin on mortality and morbidity in patients with
924 heart failure. *N Engl J Med* **336**, 525-533 (1997).

925 51 Hallberg, P., Lindbäck, J., Lindahl, B., Stenestrand, U. & Melhus, H. Digoxin and mortality in
926 atrial fibrillation: a prospective cohort study. *European journal of clinical pharmacology* **63**,
927 959-971 (2007).

928 52 Patel, N. J. *et al.* Digoxin significantly improves all-cause mortality in atrial fibrillation patients
929 with severely reduced left ventricular systolic function. *Int J Cardiol* **169**, e84-86 (2013).

930 53 Rana, S., Prabhu, S. D. & Young, M. E. Chronobiological Influence Over Cardiovascular Function:
931 The Good, the Bad, and the Ugly. *Circ Res* **126**, 258-279 (2020).

932 54 Young, M. E. *et al.* Cardiomyocyte-specific BMAL1 plays critical roles in metabolism, signaling,
933 and maintenance of contractile function of the heart. *J Biol Rhythms* **29**, 257-276 (2014).

934 55 Tsimakouridze, E. V. *et al.* Chronomics of pressure overload-induced cardiac hypertrophy in
935 mice reveals altered day/night gene expression and biomarkers of heart disease. *Chronobiol*
936 *Int* **29**, 810-821 (2012).

937 56 Carter, E. L., Ramirez, Y. & Ragsdale, S. W. The Heme Regulatory Motif of Nuclear Receptor
938 Rev-erbbeta is a Key Mediator of Heme and Redox Signaling in Circadian Rhythm Maintenance
939 and Metabolism. *J Biol Chem* **292**, 11280-11299 (2017).

940 57 Wang, J. & Lazar, M. A. Bifunctional role of Rev-erbalpha in adipocyte differentiation. *Mol. Cell*
941 *Biol* **28**, 2213-2220 (2008).

942 58 Kaasik, K. & Lee, C. C. Reciprocal regulation of haem biosynthesis and the circadian clock in
943 mammals. *Nature* **430**, 467-471 (2004).

944 59 Dioum, E. M. *et al.* NPAS2: A Gas-Responsive Transcription Factor. *Science* **298**, 2385-2387
945 (2002).

946 60 Yang, J. *et al.* A novel heme-regulatory motif mediates heme-dependent degradation of the
947 circadian factor period 2. *Mol Cell Biol* **28**, 4697-4711 (2008).

948 61 Reitz, C. J. *et al.* SR9009 administered for one day after myocardial ischemia-reperfusion
949 prevents heart failure in mice by targeting the cardiac inflammasome. *Communications*
950 *Biology* **2**, 353 (2019).

951 62 Mia, S. *et al.* Differential effects of REV-ERBalpha/beta agonism on cardiac gene expression,
952 metabolism, and contractile function in a mouse model of circadian disruption. *Am J Physiol*
953 *Heart Circ Physiol* **318**, H1487-H1508 (2020).

954 63 Zhang, L. *et al.* REV-ERB α ameliorates heart failure through transcription repression. *JCI Insight*
955 **2**, e95177 (2017).

956 64 Stujanna, E. N. *et al.* Rev-erb agonist improves adverse cardiac remodeling and survival in
957 myocardial infarction through an anti-inflammatory mechanism. *PLoS One* **12**, e0189330
958 (2017).

959 65 Zhao, Y. *et al.* Disruption of Circadian Rhythms by Shift Work Exacerbates Reperfusion Injury
960 in Myocardial Infarction. *J Am Coll Cardiol* **79**, 2097-2115 (2022).

961 66 Busonero, C. *et al.* Ouabain and Digoxin Activate the Proteasome and the Degradation of the
962 ERalpha in Cells Modeling Primary and Metastatic Breast Cancer. *Cancers (Basel)* **12**, 3840
963 (2020).

964 67 Wang, Y. *et al.* Bufalin is a potent small-molecule inhibitor of the steroid receptor coactivators
965 SRC-3 and SRC-1. *Cancer Res* **74**, 1506-1517, doi:10.1158/0008-5472.Can-13-2939 (2014).

966 68 Woldt, E. *et al.* Rev-erb-alpha modulates skeletal muscle oxidative capacity by regulating
967 mitochondrial biogenesis and autophagy. *Nat Med* **19**, 1039-1046 (2013).

968 69 Bell, R. M., Mocanu, M. M. & Yellon, D. M. Retrograde heart perfusion: the Langendorff
969 technique of isolated heart perfusion. *J Mol Cell Cardiol* **50**, 940-950 (2011).

970 70 Schmittgen, T. D. & Livak, K. J. Analyzing real-time PCR data by the comparative CT method.
971 *Nature Protocols* **3**, 1101-1108 (2008).

972 71 Harris, V. M. Protein detection by Simple Western™ analysis. *Methods Mol Biol* **1312**, 465-468
973 (2015).

974 72 Berthier, A. *et al.* Combinatorial regulation of hepatic cytoplasmic signaling and nuclear
975 transcriptional events by the OGT/REV-ERBalpha complex. *Proc Natl Acad Sci U S A* **115**,
976 E11033-E11042 (2018).

977 73 Kondo, K., Klco, J., Nakamura, E., Lechpammer, M. & Kaelin, W. G., Jr. Inhibition of HIF is
978 necessary for tumor suppression by the von Hippel-Lindau protein. *Cancer Cell* **1**, 237-246
979 (2002).

980 74 Vandell, J. *et al.* GIANT: galaxy-based tool for interactive analysis of transcriptomic data.
981 *Scientific Reports* **10**, 19835 (2020).

982 75 Hughes, M. E., Hogenesch, J. B. & Kornacker, K. JTK_CYCLE: an efficient nonparametric
983 algorithm for detecting rhythmic components in genome-scale data sets. *J Biol Rhythms* **25**,
984 372-380 (2010).

985 76 Huang da, W., Sherman, B. T. & Lempicki, R. A. Systematic and integrative analysis of large
986 gene lists using DAVID bioinformatics resources. *Nat Protoc* **4**, 44-57 (2009).

987 77 Perez-Riverol, Y. *et al.* The PRIDE database resources in 2022: a hub for mass spectrometry-
988 based proteomics evidences. *Nucleic Acids Res* **50**, D543-d552 (2022).

989

SUPPLEMENTAL DATA

990
991

992 **Extended data Fig. 1. Rhythmic gene and protein level in mouse heart whole tissue extracts. (a)**
993 WES analysis of REV-ERB α protein level in mouse hearts collected over a 24-hours period at rest phase
994 (ZT0-ZT12) and active phase (ZT13-ZT24) (n=4). HSP90 α was used as a protein loading control. **(b)**
995 WES analysis of REV-ERB α protein level in mouse hearts collected at ZT9 after vehicle or digoxin
996 injection (0.1,0.5, and 0.1mpk at ZT5. **(c)** Cyclic *Nr1d1*, *Nr1d2*, *Bmal1* and *Cdkn1a* mRNA expression in
997 mouse hearts collected at rest (ZT0-ZT12) or active (ZT13-ZT24) phases Results are shown as mean+/-
998 SEM (n=3). **(d)** *Nr1d1*, *Arntl* (*Bmal1*) and *Cdkn1a* mRNA expression in mouse hearts collected at ZT9
999 after vehicle or digoxin (1mpk) injection at ZT5. Results are shown as mean+/-SEM (n=8-9) which were
1000 compared using which were compared using a two-tailed Welch's t-test. **(e)** P21 protein level in mouse
1001 hearts collected at ZT9 after vehicle or digoxin (1mpk) injection at ZT5. **(f)** REV-ERB α protein level in
1002 mouse hearts collected at ZT0 after vehicle or digoxin (1mpk) injection at ZT20. Basal REV-ERB α
1003 protein level at ZT9 is shown here as reference. Measurements were from distinct samples.
1004 Quantification of data in panels (a), (b) and (c) appears in Fig. 1.

1005 **Extended data Fig. 2. NKA status in mouse heart and AC16 cells. (a)** Left panel: NKA isotype-encoding
1006 mRNA expression in mouse heart. *Atp1a1*, *Atp1a2* and *Atp1a3* expression levels are plotted as a
1007 function of time. *Per1* mRNA expression is shown as a reference circadian gene. Middle panel: Relative
1008 expression of NKA isotype-encoding mRNA expression in mouse heart at ZT9. Results are shown as
1009 mean+/-SEM (n=8-15) which were compared using Brown-Forsythe & Welch ANOVA test, followed by
1010 Dunnett's multiple comparison test. Right panel: Effect of digoxin treatment on NKA isotype-encoding
1011 mRNA expression in mouse heart at ZT9. Results are shown as mean+/-SEM (n=8-15) which were
1012 compared using Brown-Forsythe & Welch ANOVA test, followed by Dunnett's multiple comparison
1013 test. **(b)** NKA isotype protein expression level in mouse heart as a function of time. Data quantification
1014 is shown (right panel) as mean+/-SEM (n=3) which were compared using a one-way ANOVA test,
1015 followed by a Tukey's multiple comparison test. *: P<0.05, **: P<0.01, ***: P<0.001. **(c)** Left panel:
1016 Relative expression of NKA isotype-encoding mRNA expression in human AC16 cells (T₂₄). Right panel:
1017 Effect of digoxin treatment on NKA isotype-encoding mRNA expression in human AC16 cells (T₂₄).
1018 Results are shown as mean+/-SEM (n=5-6) which were compared using a one-way ANOVA test,
1019 followed by a Tukey's multiple comparison test. **(d)** NKA isotype protein expression level in human
1020 AC16 as a function of time. Data quantification is shown (right panel) as mean+/-SEM (n=4) which
1021 were compared using a one-way ANOVA test, followed by a Tukey's multiple comparison test. All
1022 measurements were from distinct samples. *: P<0.05, **: P<0.01

1023 **Extended data Fig. 3. Effects of digoxin and of its structural analogs on REV-ERB α protein stability.**
1024 **(a)** AC16 cellular viability in the presence of increasing concentrations of digoxin. Data are plotted as
1025 mean \pm -SEM (n=4) which were compared using a one-way ANOVA test, followed by a Tukey's multiple
1026 comparison test. **(b)** Protein array analysis of AC16 whole cell protein extract. AC16 cells were treated
1027 for 6hours at T₁₈ as indicated and extracts were probed on membrane spotted with antibodies specific
1028 for components of the apoptotic pathway. Fluorescence signals were quantified and were represented
1029 as a heatmap (n=2). **(c)** Cyclic REV-ERB α protein levels in human AC16 cells. REV-ERB α levels were
1030 determined in synchronized human AC16 cells treated with vehicle or digoxin (0.5 μ M) and harvested
1031 at T₀, T₆, T₁₂, T₁₈ and T₂₄. Quantification of data is shown in Fig. 2A. **(d)** REV-ERB α protein level was
1032 assessed in AC16 cells treated with vehicle, digoxin (0.5 μ M) and/or DigiFab (100 μ g). HSP90 α was used
1033 as a protein loading control. Right panel: normalized data are plotted as mean \pm -SEM (n=3) which
1034 were compared using a one-way ANOVA test, followed by a Tukey's multiple comparison test. **(e)** REV-
1035 ERB α protein level was assessed in AC16 cells treated with vehicle or varying concentration of digoxin
1036 as indicated. HSP90 α was used as a protein loading control Right panel: normalized data are plotted
1037 as mean \pm -SEM (n=3) and analyzed by nonlinear regression curve fitting. **(f)** REV-ERB α protein level in
1038 AC16 cells treated with vehicle or varying concentrations of bufalin (0.1, 1.0, 10 μ M) (n=2). **(g)** REV-
1039 ERB α protein level in AC16 cells treated with vehicle or ouabain (5 μ M) (n=2). HSP90 α was used as a
1040 protein loading control. All measurements were from distinct samples. **(h)** Time course experiment
1041 in AC16 cells treated at T₁₈ with vehicle or digoxin (5 μ M). REV-ERB α protein level was assessed using
1042 the ProteinSimple Wes system (n=2). HSP90 α was used as a protein loading control. All measurements
1043 were from distinct samples. ***: P<0.001.

1044 **Extended data Fig. 4. Digoxin effect in U2OS cells. (a)** Rhythmic REV-ERB α and ROR α protein level in
1045 synchronized U2OS cells treated with vehicle or digoxin (0.5 μ M) and harvested over a 36-hour period
1046 as indicated. HSP90 α was used as a protein loading control. **(b)** *NR1D1* and *BMAL1* mRNA expression
1047 in synchronized U2OS cells treated with vehicle or digoxin (0.5 μ M) and harvested at T₂₄. Normalized
1048 data are plotted as mean \pm -SEM (n=6) which were compared using a one-way ANOVA test, followed
1049 by a Tukey's multiple comparison test. **(c)** Bioluminescent signal in U2OS cells transfected with the
1050 *Bmal1*-Luc plasmid and treated with vehicle or digoxin (0.5 μ M). Detrended data are shown HSP90 α
1051 was used as a protein loading control. All measurements were from distinct samples.

1052 **Extended data Fig. 5. Effect of protein kinase inhibition or activation on digoxin-mediated REV-ERB α**
1053 **protein level decrease.** Representative WES analysis (related to quantified data in Fig. 4) are shown.
1054 REV-ERB α protein level in synchronized AC16 cells treated with REV-ERB α protein levels were
1055 quantified after a 6 hour-treatment with or without digoxin and with or without enzyme inhibitors: **(a)**

1056 PP2 (20μM, Src kinase inhibitor), **(b)** ZSTK474 (10μM, PI3 kinase inhibitor), **(c)** SCH772984 (10μM, ERK
1057 1&2 inhibitor), **(d)** MK2206 (1μM, AKT1/2/3 kinase inhibitor), **(e)** KN93 (10μM, CAMK 2&4 inhibitor),
1058 **(f)** PD98059 (10μM, MEK 1&2 inhibitor), **(g)** RP-8-pCPT-cGMPs (20μM, PKG1&2), **(h)** CRT0066101
1059 (5μM, PKD inhibitor), **(i)** PF-4708671 (10μM, P70S6K1 inhibitor), **(j)** BAY11-7082 (10μM, LUBAC and
1060 UPS inhibitor), **(k)** HOIPIN8 (10μM, LUBAC-HOIP specific inhibitor), **(l)** TPCA-1 (20nM, IKKβinhibitor),
1061 **(m)** TPCA-1 (5μM, IKKβ/α inhibitor) **(n)** amlexanox (1μM, IKKε & TBK1 inhibitor). HSP90α was used as
1062 a protein loading control.

1063 **Extended data Fig. 6. Effect of protein kinase inhibition or activation on digoxin-mediated REV-ERBα**
1064 **protein level decrease.** Quantification of REV-ERBα protein levels in synchronized human AC16 cells
1065 (see Extended data Fig. 7) **(a)** treated with vehicle, digoxin (0.5μM) and/or SRC inhibitor (saracatinib),
1066 **(b)** treated with vehicle, digoxin (0.5μM) and/or PI3K inhibitor (LY294002) **(c)** treated with vehicle,
1067 digoxin (0.5μM) and/or PI3K/P70S6K inhibitor (dactolisib), **(d)** transfected with ERK1 expression vector,
1068 **(e)** treated with the GSK3β inhibitor lithium and/or digoxin, **(f)** transfected with scrambled siRNA (Scr
1069 siRNA) or *CAMK4* siRNA and treated with vehicle or digoxin (0.5μM), **(g)** transfected with scrambled
1070 siRNA (Scr siRNA) or *ERK1&3* siRNA and treated with vehicle or digoxin (0.5μM), **(h)** transfected with
1071 scrambled siRNA (Scr siRNA) or *PKD1* siRNA and treated with vehicle or digoxin (0.5μM), **(i)** transfected
1072 with scrambled siRNA (Scr siRNA) or *PRKG1* siRNA and treated with vehicle or digoxin (0.5μM), **(j)**
1073 transfected with scrambled siRNA (Scr siRNA) or *HOIL* siRNA and treated with vehicle or digoxin
1074 (0.5μM) and **(k)** transfected with an empty (pcDNA3) or OTULIN-expressing (pcDNA3-*OTULIN*) vector
1075 and treated with vehicle or digoxin (0.5μM). Normalized data are plotted as mean+/-SEM (n=3-6) and
1076 compared using a one-way ANOVA test, followed by a Tukey's multiple comparison test except for **(c)**
1077 for which groups were compared using an unpaired 2-tailed *t*-test. All measurements were from
1078 distinct samples.

1079 **Extended data Fig. 7. Effect of protein kinase inhibition or activation on digoxin-mediated REV-ERBα**
1080 **protein level decrease.** WES analysis of REV-ERBα protein levels in synchronized human AC16 cells **(a)**
1081 treated with vehicle, digoxin (0.5μM) and/or SRC inhibitor (saracatinib, 10μM), **(b)** treated with vehicle,
1082 digoxin (0.5μM) and/or PI3K inhibitor (LY294002, 20μM) **(c)** treated with vehicle, digoxin (0.5μM)
1083 and/or PI3K/P70S6K inhibitor (dactolisib, 0.1μM), **(d)** transfected with ERK1 expression vector, **(e)**
1084 treated with the GSK3β inhibitor lithium (20mM) and/or digoxin, **(f)** transfected with scrambled siRNA
1085 (Scr siRNA) or *CAMK4* siRNA and treated with vehicle or digoxin (0.5μM), **(g)** transfected with
1086 scrambled siRNA (Scr siRNA) or *ERK1&3* siRNA and treated with vehicle or digoxin (0.5μM), **(h)**
1087 transfected with scrambled siRNA (Scr siRNA) or *PKD1* siRNA and treated with vehicle or digoxin
1088 (0.5μM), **(i)** transfected with scrambled siRNA (Scr siRNA) or *PKG1* siRNA and treated with vehicle or
1089 digoxin (0.5μM), **(j)** transfected with scrambled siRNA (Scr siRNA) or *HOIL* siRNA and treated with

1090 vehicle or digoxin (0.5 μ M) and **(k)** transfected with an empty (pcDNA3) or OTULIN-expressing
1091 (pcDNA3-*OTULIN*) vector and treated with vehicle or digoxin (0.5 μ M).

1092 **Extended data Fig. 8. Proteasome inhibition counteracts digoxin effect on REV-ERB α levels.**

1093 Quantification of data appears in Fig. 5. REV-ERB α protein level in synchronized AC16 cells **(a)** treated
1094 with either vehicle, digoxin (0.5 μ M) and/or clasto-lactacystin β -lactone (10 μ M, proteasomal inhibitor),
1095 **(b)** treated with either vehicle, digoxin (0.5 μ M) and/or bortezomib (200nM, PSMB5 inhibitor), in
1096 synchronized U2OS cells treated **(c)** with either vehicle, digoxin (0.5 μ M) and/or bortezomib (200nM,
1097 PSMB5 inhibitor) in synchronized AC16 cells **(d)** in synchronized AC16 cells transfected with Flag-Rev-
1098 ERB α or Flag-Rev-ERB α -H602F then treated with vehicle or digoxin (0.5 μ M). HSP90 α was used as a
1099 protein loading control.

1100 **Extended data Fig. 9. Screening E2/E3 ligases potentially involved in digoxin-induced REV-ERB α**

1101 **degradation. (a)** Quantification of REV-ERB α protein level in AC16 cells transfected either with
1102 scrambled siRNA (Scr siRNA) or *SIAH2* siRNA and treated with vehicle or digoxin (0.5 μ M). A strictly
1103 identical protocol was followed to assess the effect of *FBXW7* **(b)**, *GSK3 β* **(c)**, *UBE2L3* **(d)**, *HUWE1* **(e)**,
1104 *PSME3* **(f)**, *TBL1XR1* **(g)**, *BUB3* **(h)**, *CBL*, *BRCA1*, *UBE4A* **(i)**, *UBE4B*, *MDM2*, *STUB1* **(j)**, and of *TRIM21* and
1105 *TRIM33* **(k)** knockdowns on REV-ERB α stability. Normalized data are plotted as mean \pm -SEM (n=3-6)
1106 and compared using a one-way ANOVA test, followed by a Tukey's multiple comparison test. All
1107 measurements were from distinct samples.

1108 **Extended data Fig. 10. Screening E2/E3 ligases potentially involved in digoxin-induced REV-ERB α**

1109 **degradation. (a)** REV-ERB α protein level in AC16 cells transfected either with scrambled siRNA (Scr
1110 siRNA) or *SIAH2* siRNA and treated with vehicle or digoxin (0.5 μ M). A strictly identical protocol was
1111 followed to assess the effect of *FBXW7* **(b)**, *GSK3 β* **(c)**, *UBE2L3* **(d)**, *HUWE1* **(e)**, *PSME3* **(f)**, *TBL1XR1* **(g)**,
1112 *BUB3* **(h)**, *CBL*, *BRCA1*, *UBE4A* **(i)**, *UBE4B*, *MDM2*, *STUB1* **(j)**, and of *TRIM21* and *TRIM33* **(k)** knockdowns
1113 on REV-ERB α stability.

1114 **Supplemental Dataset 1. Gene expression profiling in ZT0 vs ZT12 mouse hearts.** Mouse hearts were

1115 collected at ZT0 or ZT12 (n=7 per group) and RNAs were extracted and quantified by Affymetrix arrays.
1116 Results are expressed as fold change and corrected p values are indicated (fold-change > 1.2 with an
1117 FDR < 0.05, after a moderated t-test followed by a Benjamini-Hochberg multiple testing correction).
1118 For the sake of clarity, only protein-encoding genes are indicated.

1119 **Supplemental Dataset 2. Gene expression profiling in Nr1d1^{+/+} vs Nr1d1^{-/-} (ZT12) mouse hearts.**

1120 Mouse hearts were collected at ZT12 (n=7 per group) from Nr1d1^{+/+} vs Nr1d1^{-/-} mice and RNAs were
1121 extracted and quantified by Affymetrix arrays. Results are expressed as fold change and corrected p

1122 values are indicated (fold-change > 1.2 with an FDR < 0.05, after a moderated t-test followed by a
1123 Benjamini-Hochberg multiple testing correction). For the sake of clarity, only protein-encoding genes
1124 are indicated.

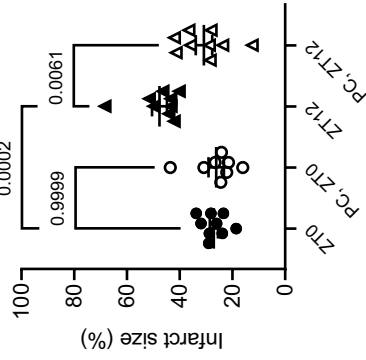
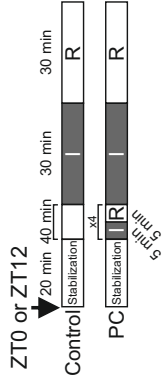
1125 **Supplemental Dataset 3. Transcriptomic alterations in digoxin-treated AC16 cells.** AC16 cells were
1126 treated after synchronization by low (0.5 μ M) or high (5 μ M) digoxin concentrations (n=3). mRNA levels
1127 were quantified by Affymetrix arrays. Results are expressed as fold change and corrected p values are
1128 indicated (fold-change > 1.2 with an FDR < 0.05, after a moderated t-test followed by a Benjamini-
1129 Hochberg multiple testing correction). For the sake of clarity, only protein-encoding genes are
1130 indicated.

1131 **Supplemental Dataset 4. Transcriptomic alterations in digoxin-treated mice.** Mice were injected at
1132 ZT5 and hearts were collected at ZT9 (n=3-5). After RNA extraction, gene expression was assayed and
1133 expressed as described in Supplementary Dataset 1 (fold-change > 1.2 with an FDR < 0.05, after a
1134 moderated t-test followed by a Benjamini-Hochberg multiple testing correction). For the sake of
1135 clarity, only protein-encoding genes are indicated.

1136 **Supplementary Dataset 5. Transcriptomic alterations common to mouse heart and human AC16**
1137 **cells.** Data from Supplementary Datasets 1 and 2 were compared and common genes to both lists are
1138 indicated.

1139 **Supplementary Dataset 6. REV-ERB α RIME data.** REV-ERB α was pulled down from AC16 and HepG2
1140 cells and associated proteins were identified by LC-MS/MS (n=1 for HepG2 and n=2 for U2OS). The list
1141 of common REV-ERB α interactants is shown, with selected interactants related to UPS indicated in
1142 bold. The threshold for significant interaction was arbitrarily set to 5 detected peptides to select a
1143 testable set of interactants.

1144

a**b**

ZT12 vs ZT0

Down Up

GOTERM_BP Rhythmic Process (11/87)

GOTERM_BP Circadian regulation of gene exp. (7/87)

GOTERM_BP Circadian rhythm (8/87)

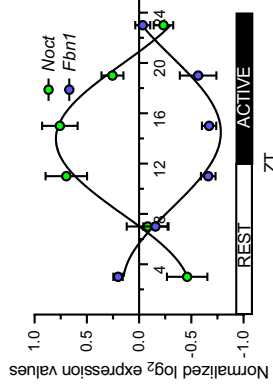
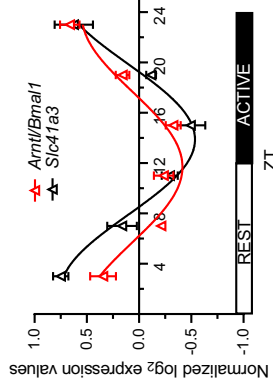
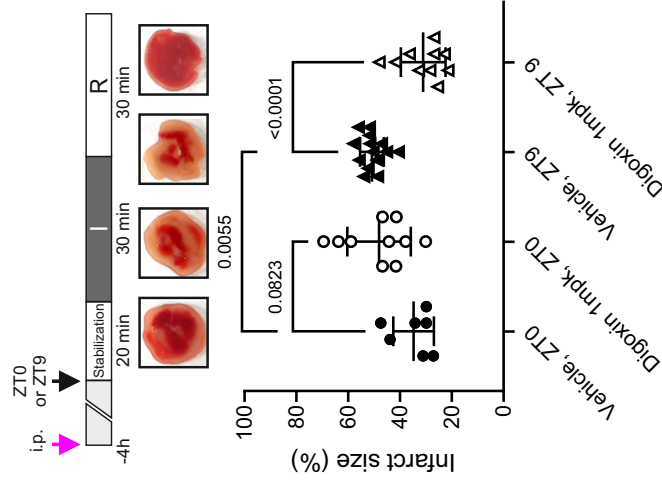
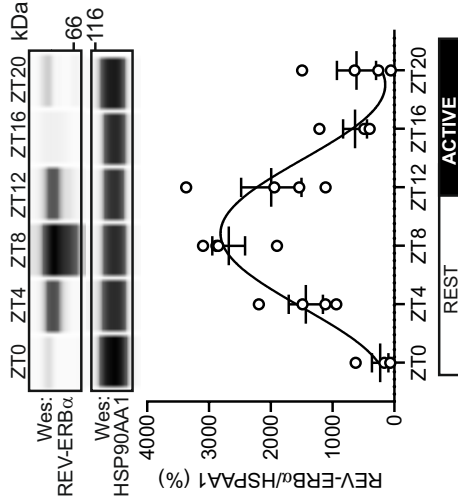
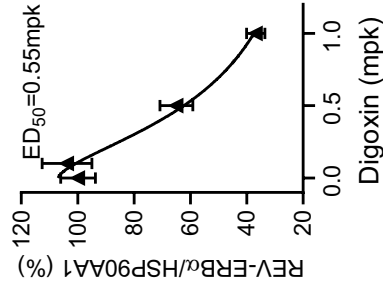
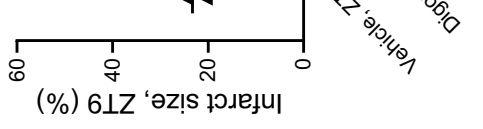
GOTERM_BP Circadian rhythm (6/58)

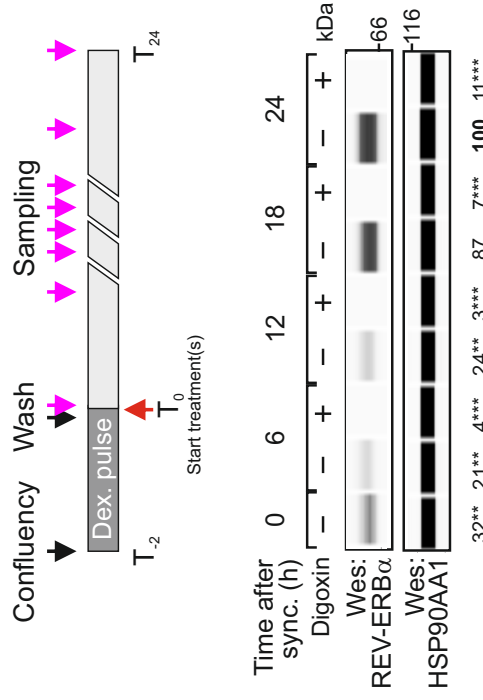
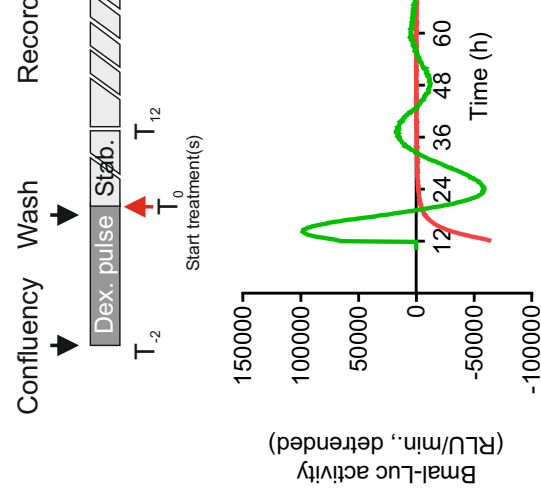
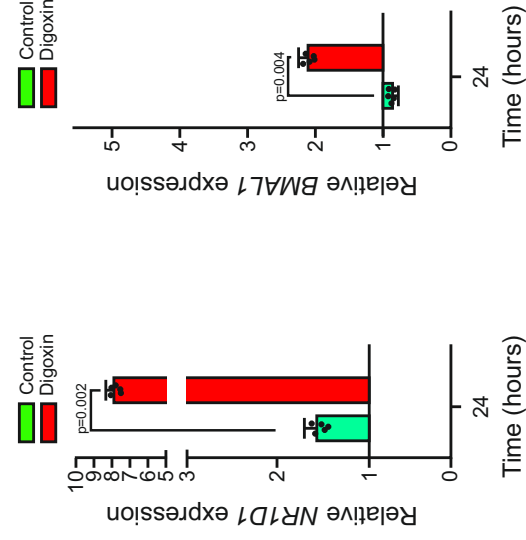
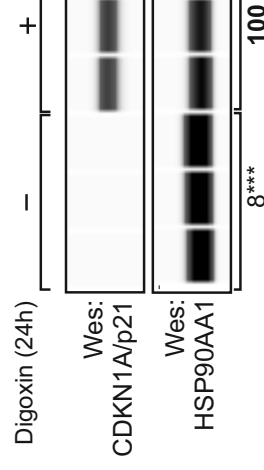
GOTERM_BP Rhythmic Process (6/58)

GOTERM_BP Response to redox state (3/58)

$-\log_{10}(\text{corr. p})$

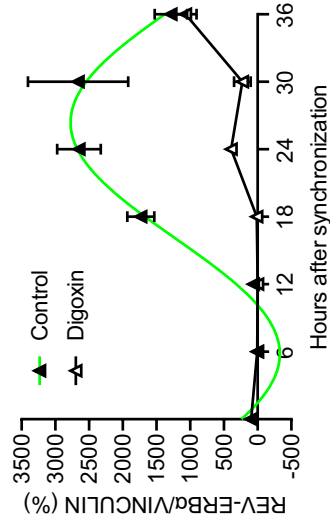
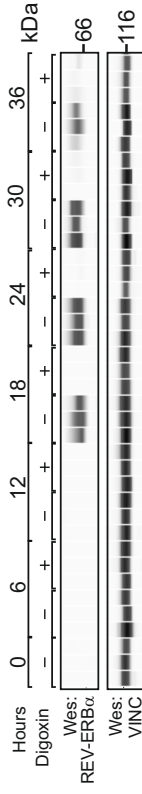
0 3.5 7.0

c**d****e****f****g**

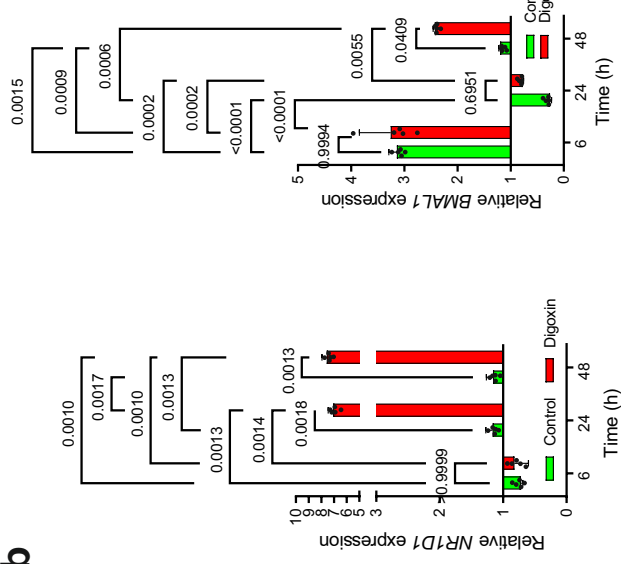
a**c****b****d**

Human primary cardiomyocytes

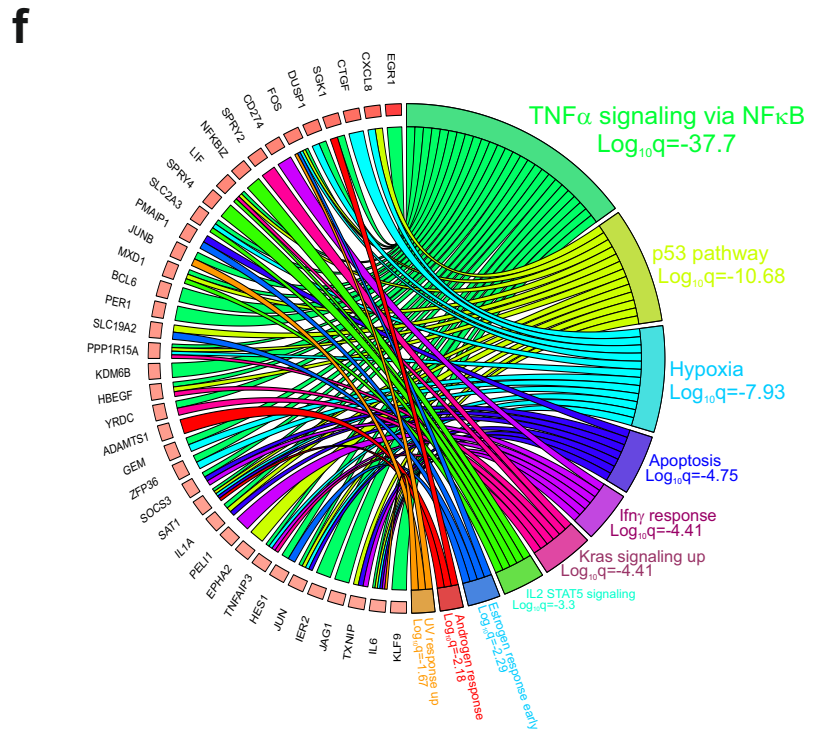
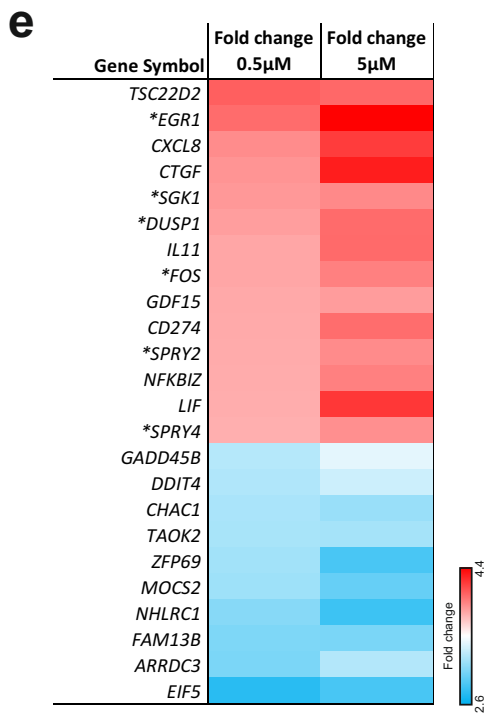
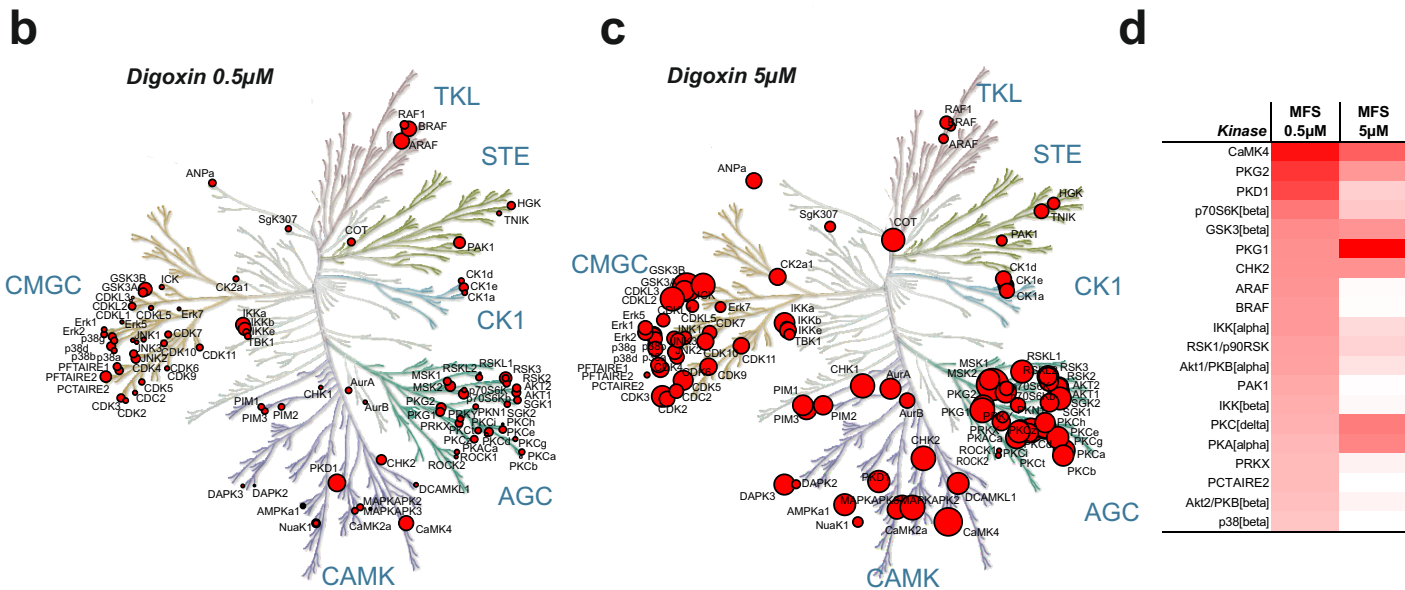
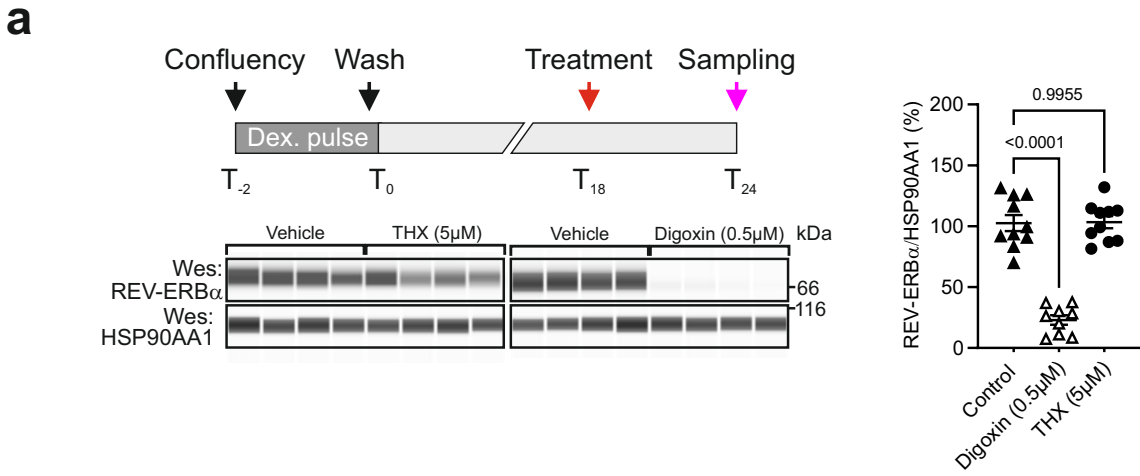
a



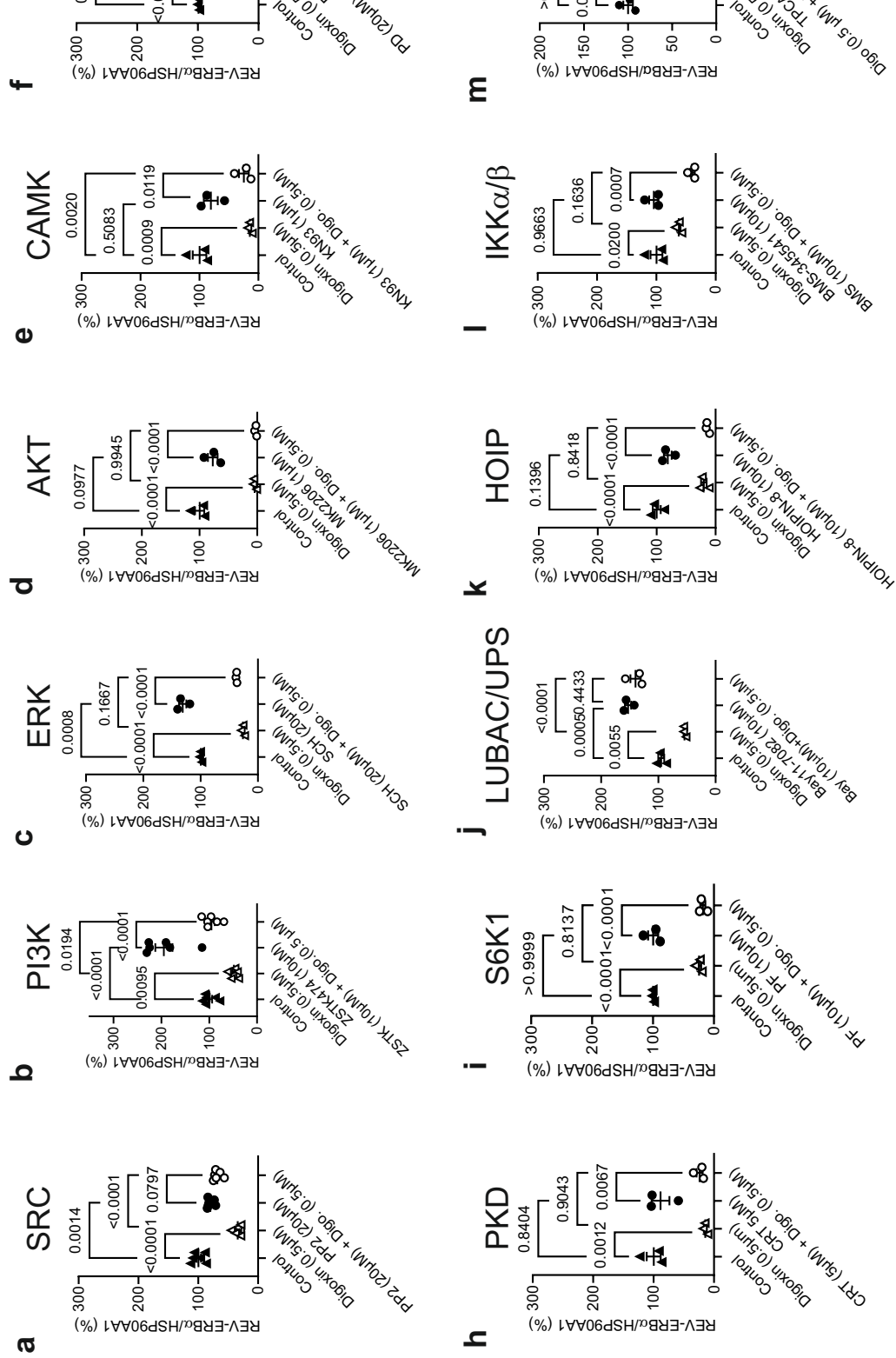
b

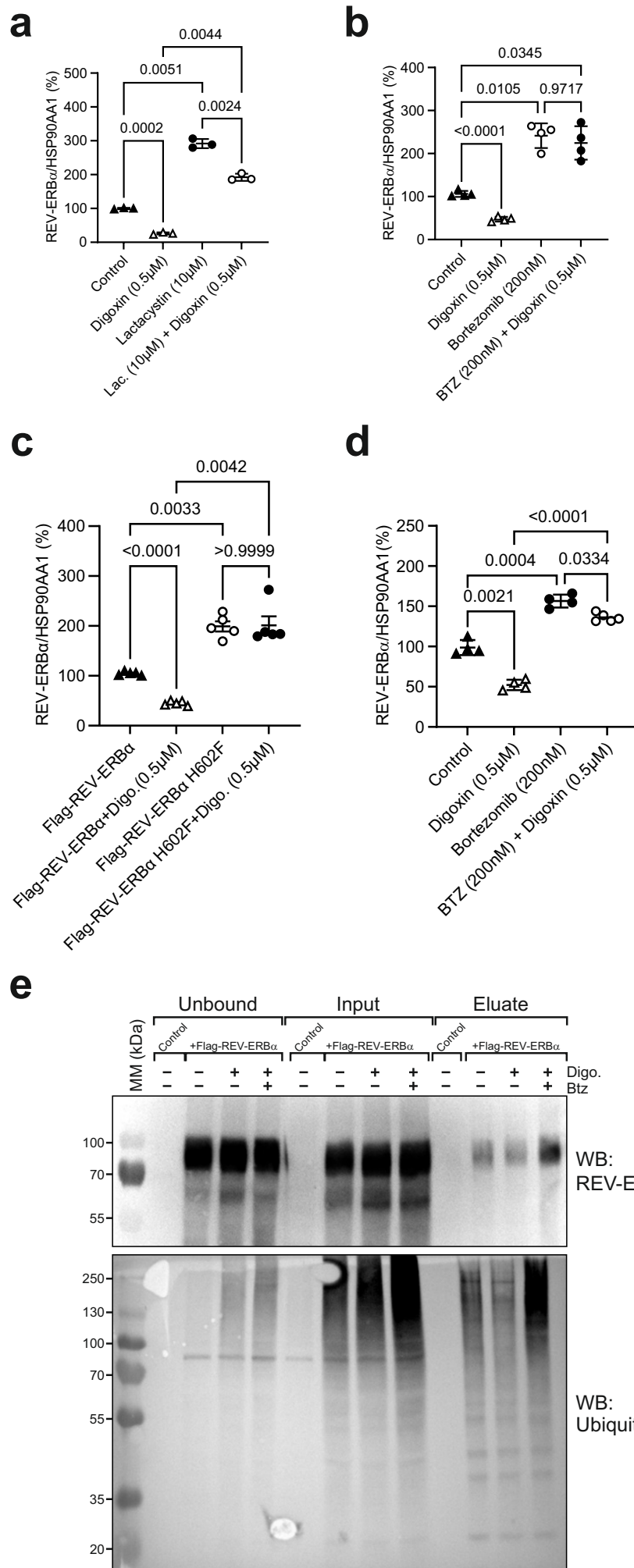


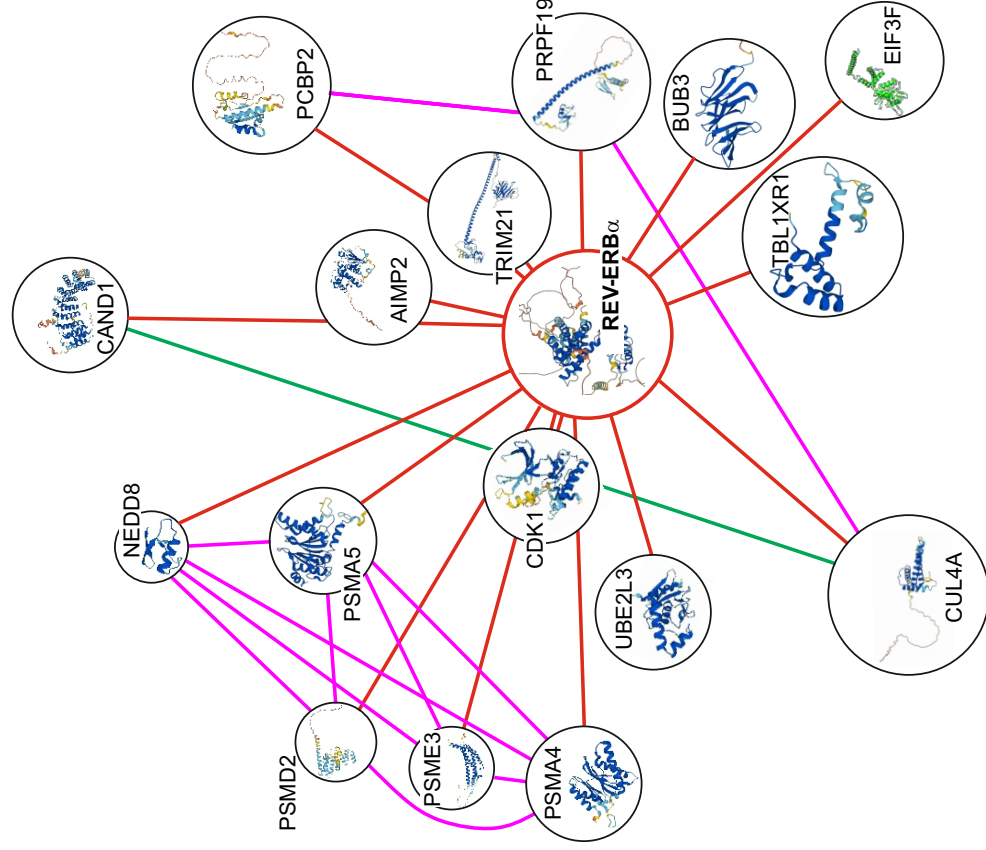
Vinod et al. - FIGURE 3



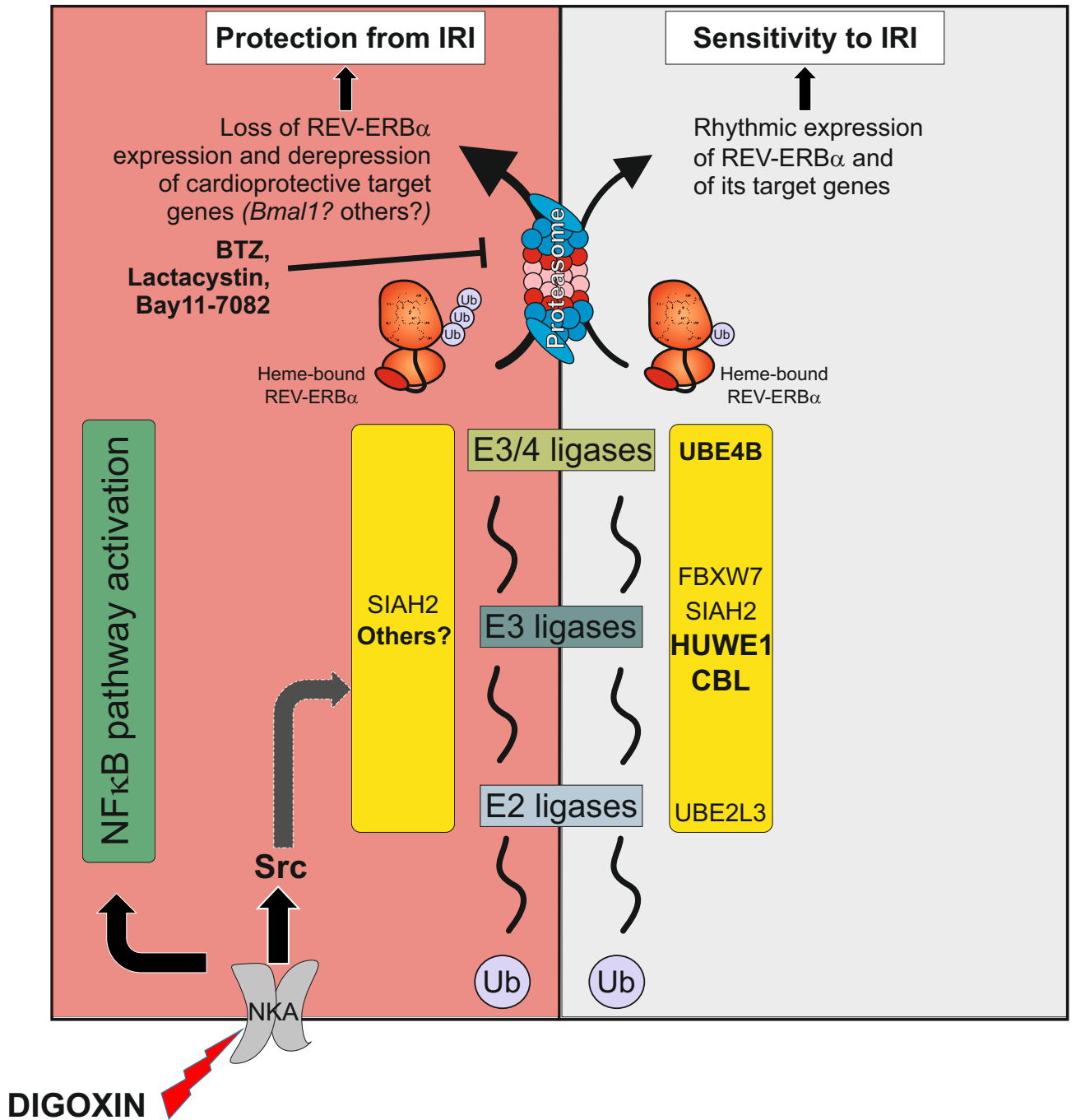
Vinod et al. - FIGURE 4



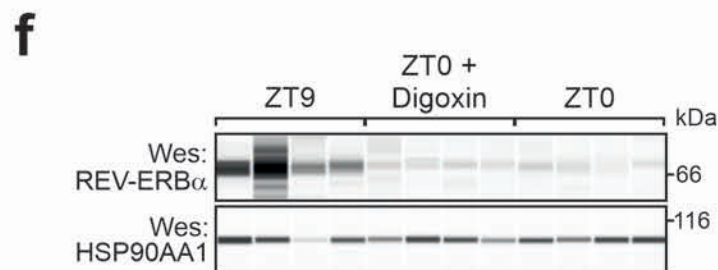
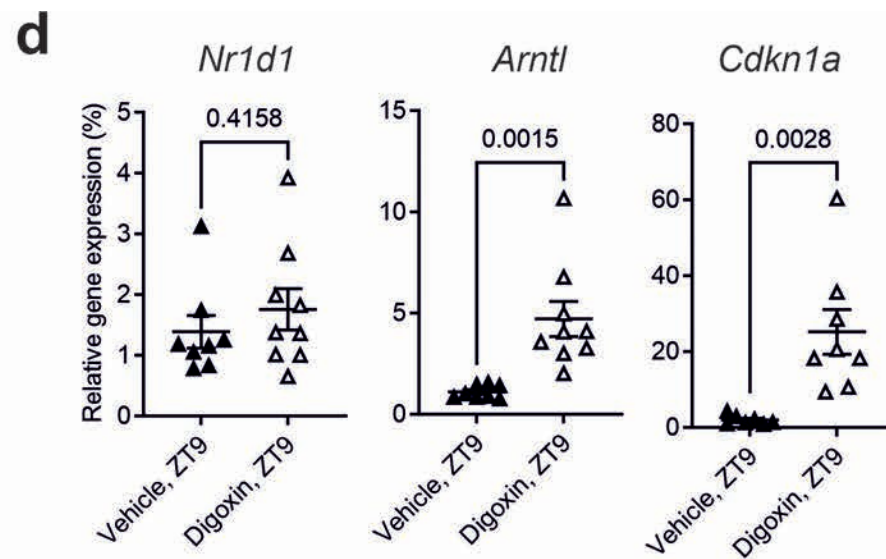
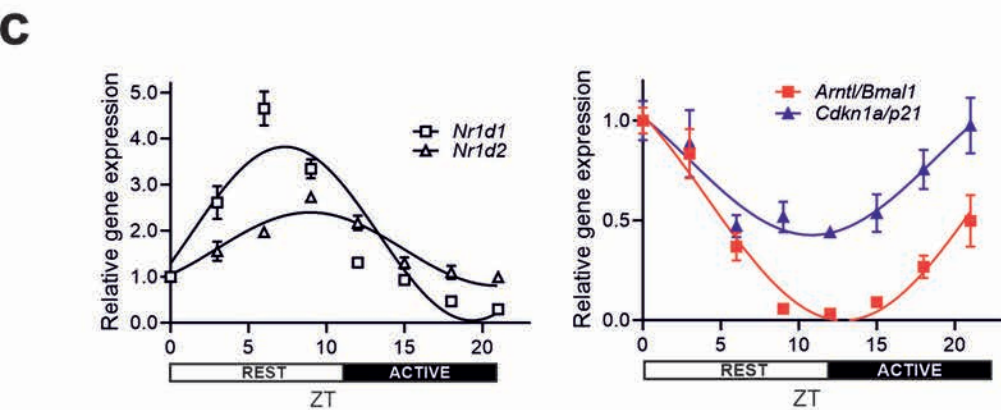
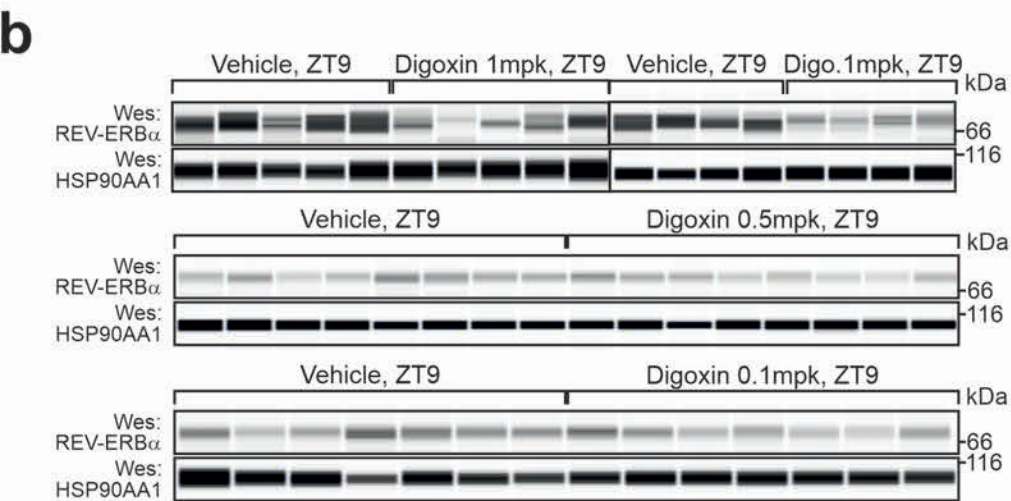
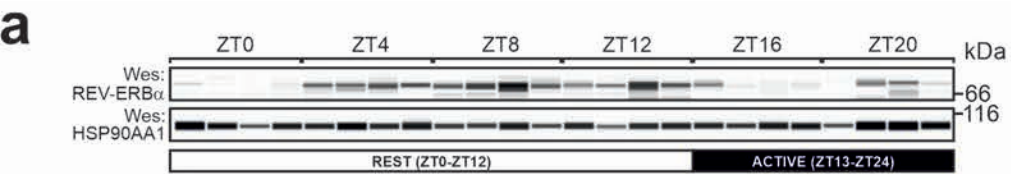


a**b**

REV-ERB α interactants	REV-ERB α	REV-ERB α
NEDD8	█	█
PSMD2	█	█
PSMA5	█	█
PSME3	█	█
PSMA4	█	█
UBE2L3	█	█
CUL4A	█	█
CAND1	█	█
TBL1XR1	█	█
CDK1	█	█
AIMP2	█	█
TRIM21	█	█
EIF3F	█	█
BUB3	█	█
PRPF19	█	█
PCBP2	█	█
SIAH2	█	█
FBXW7	█	█
GSK3 β	█	█
CBL	█	█
BRCA1	█	█
UBE4A	█	█
UBE4B	█	█
MDM2	█	█
STUB1	█	█
TRIM33	█	█
HUWE1	█	█
PSMB5	█	█

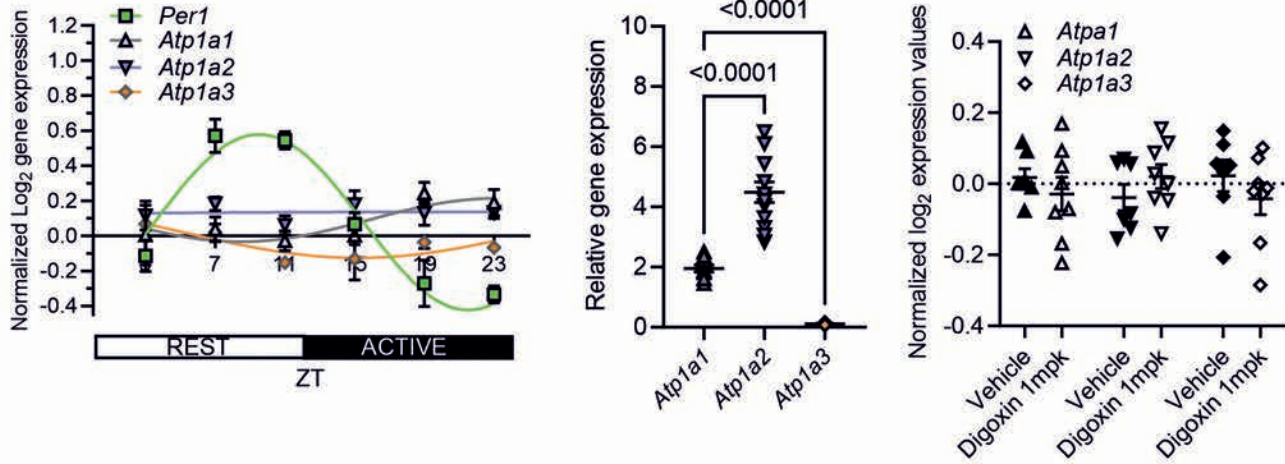


Vinod et al. - FIGURE 8

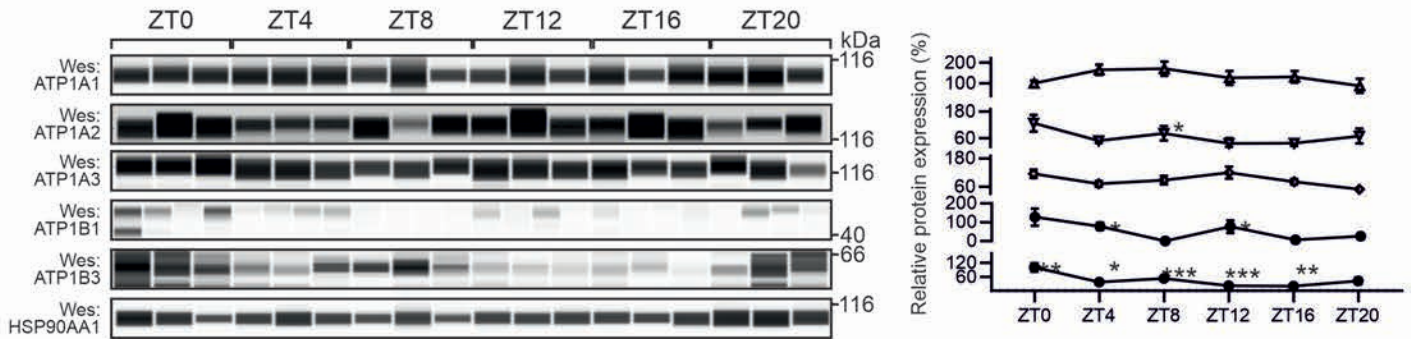


Mouse heart

a

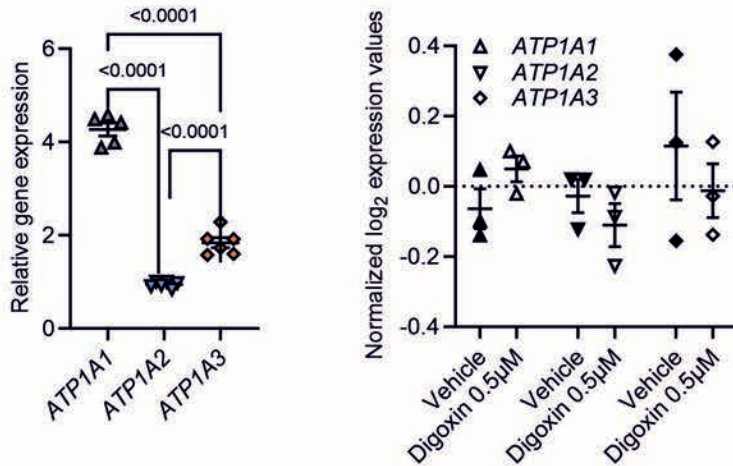


b

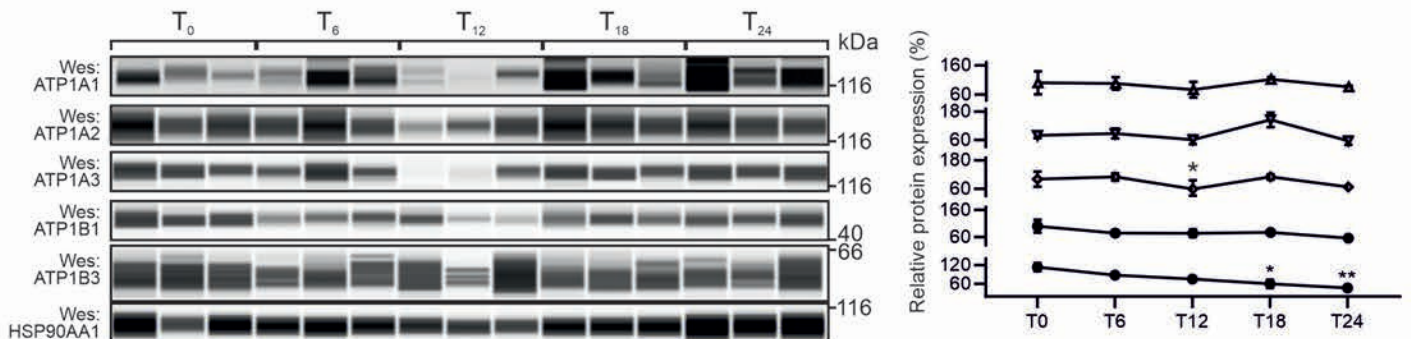


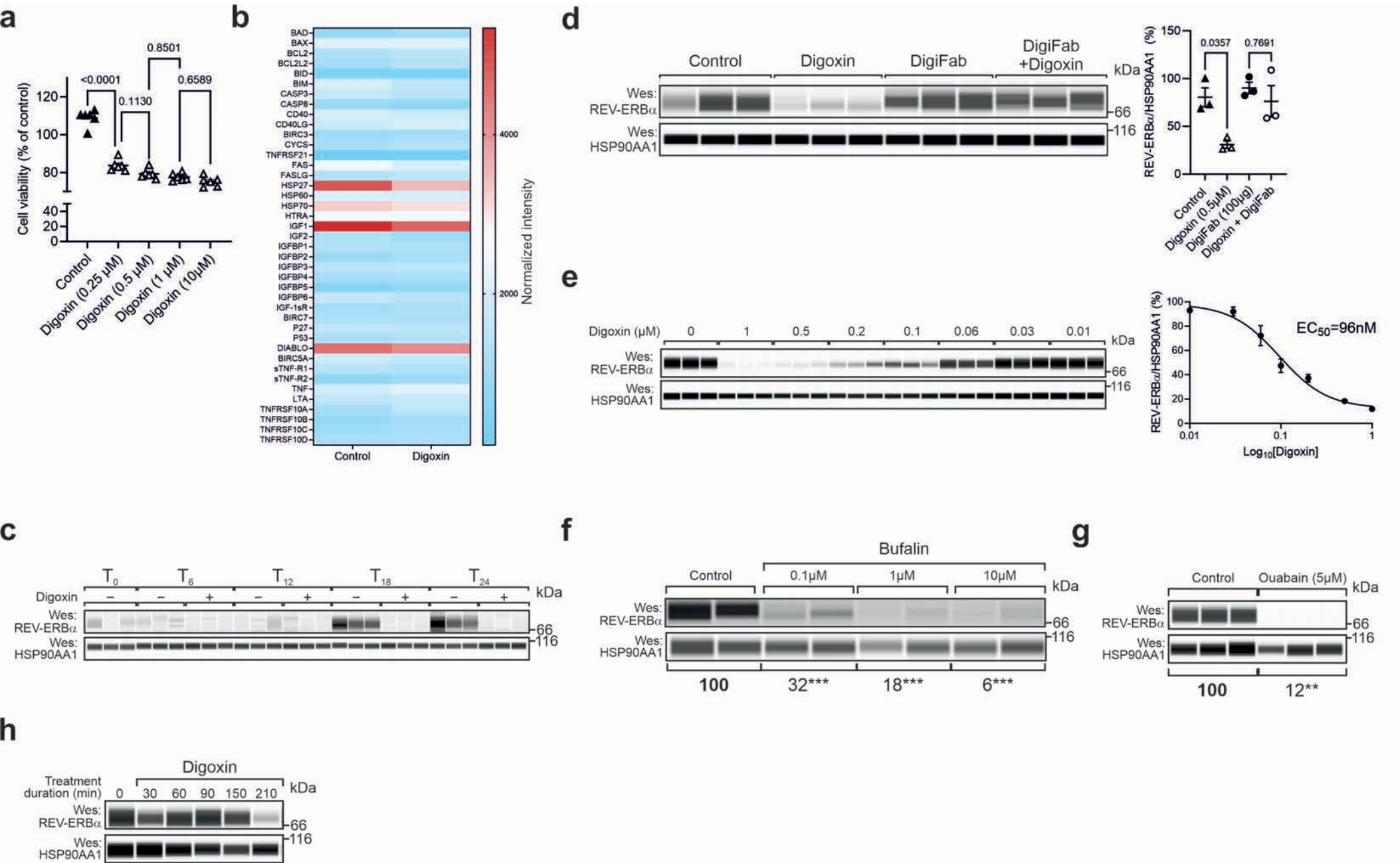
AC16 human cells

c



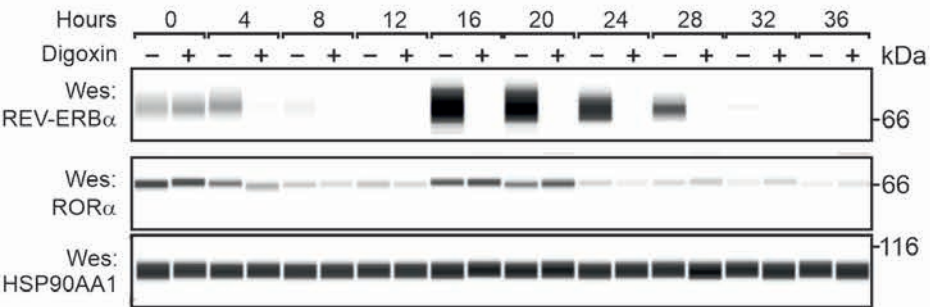
d



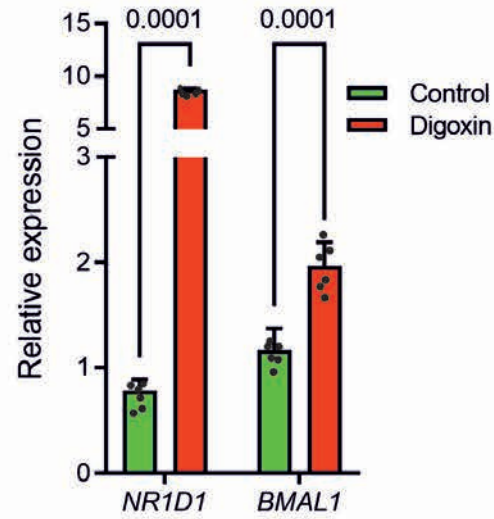


Human osteosarcoma U2OS cells

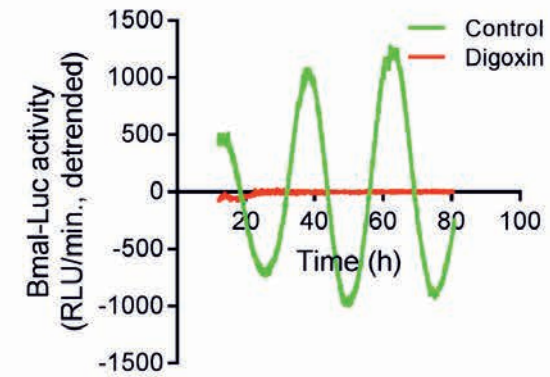
a

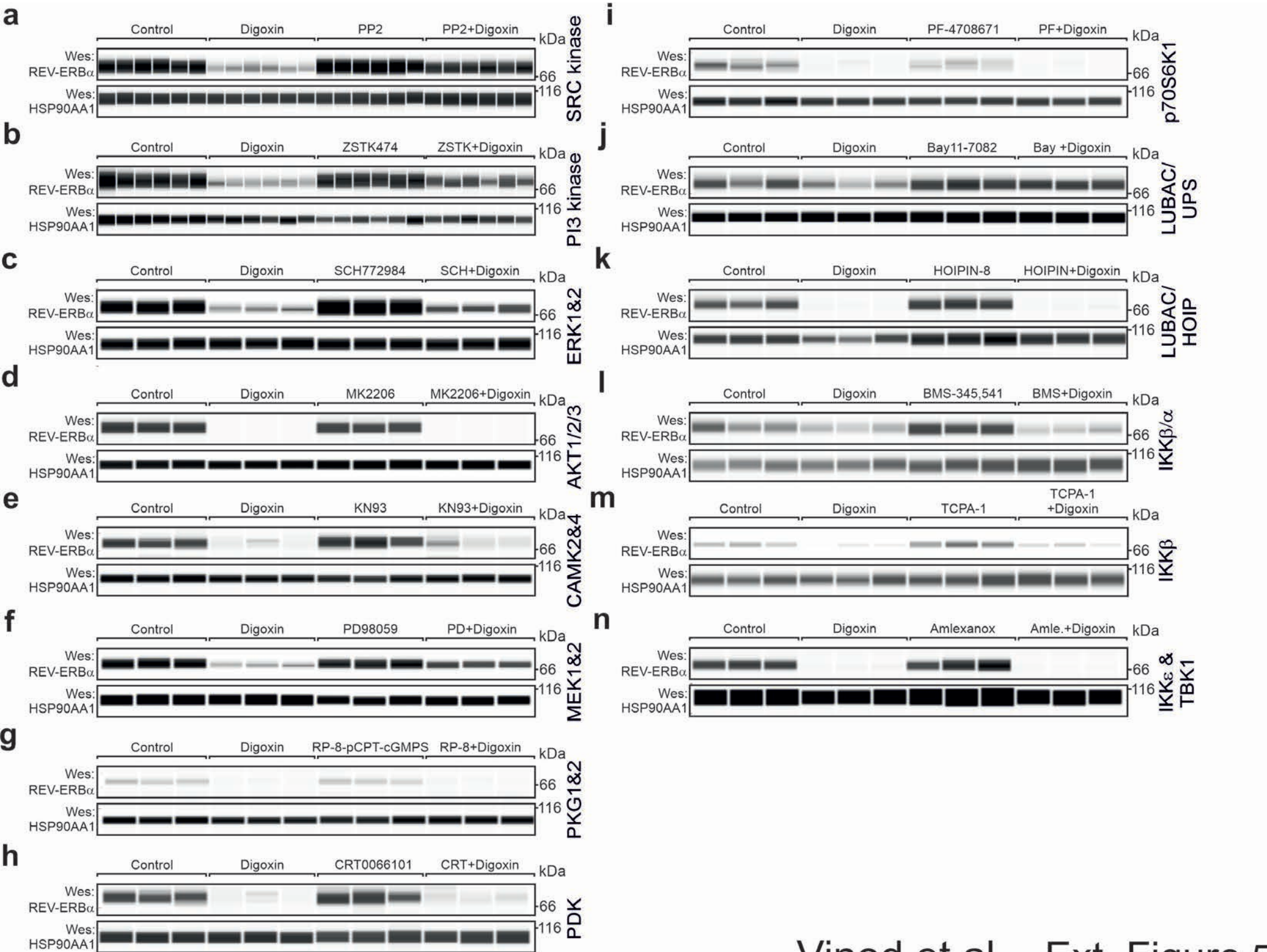


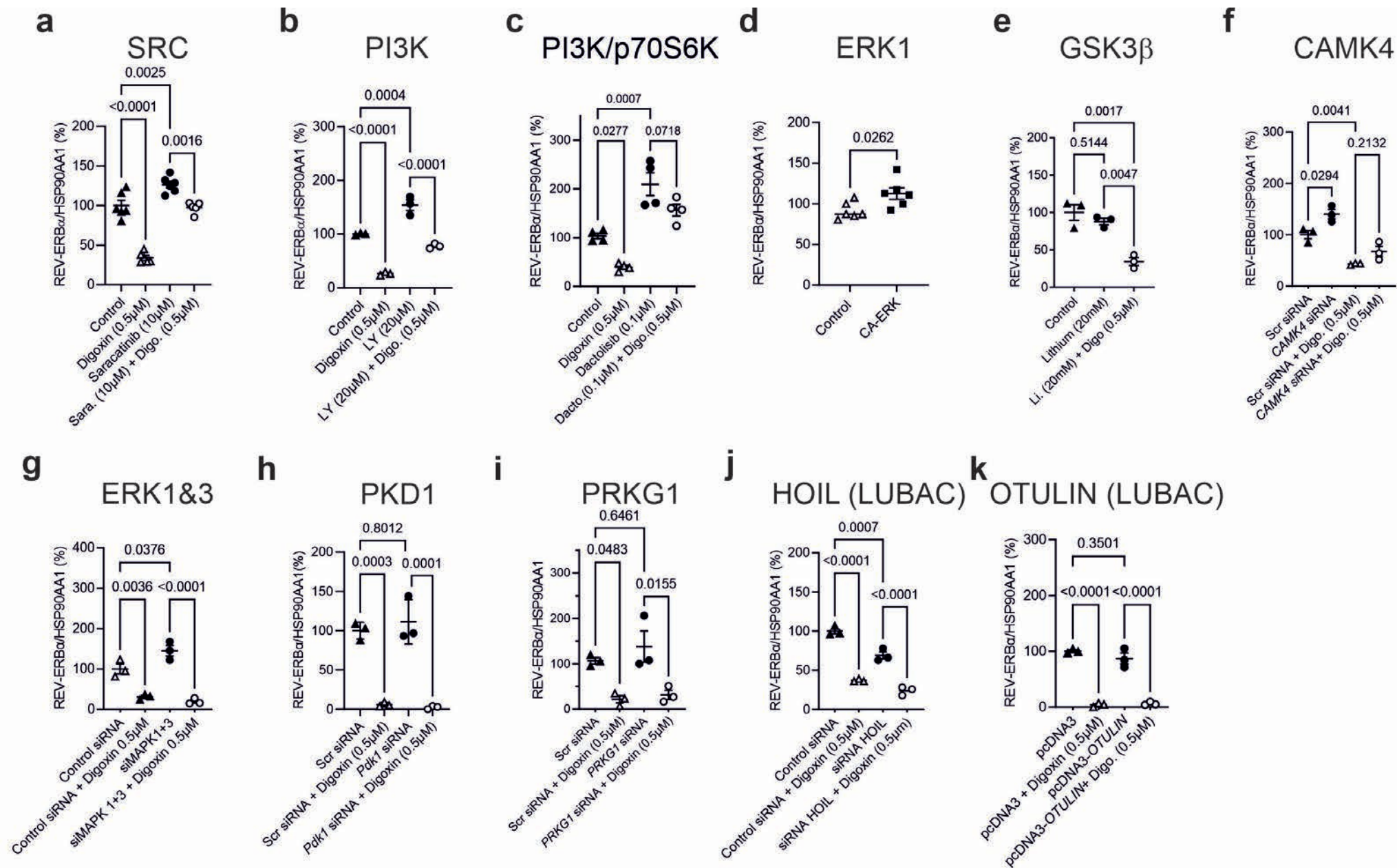
b



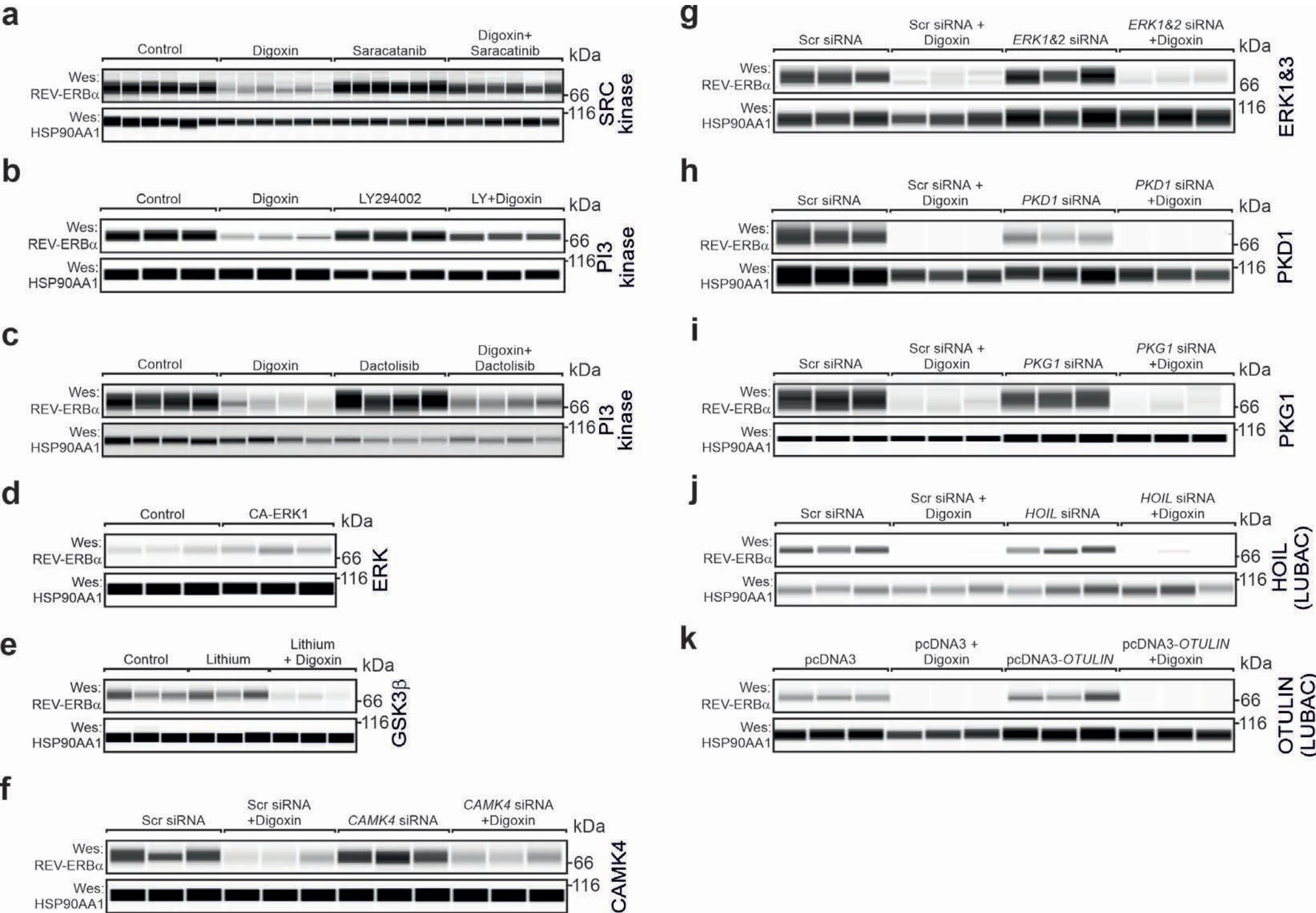
c

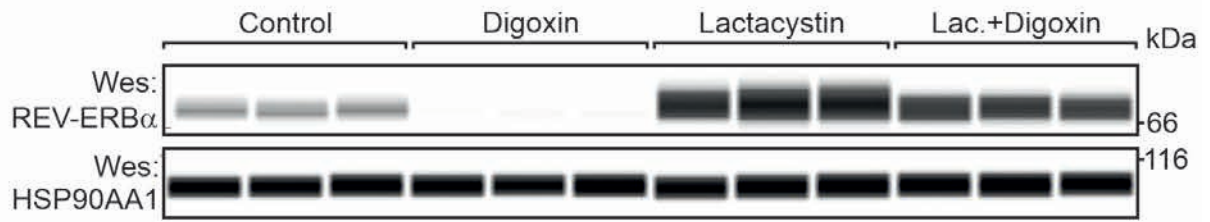
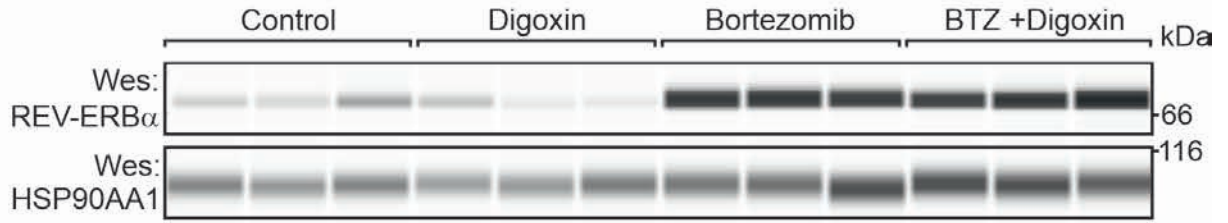
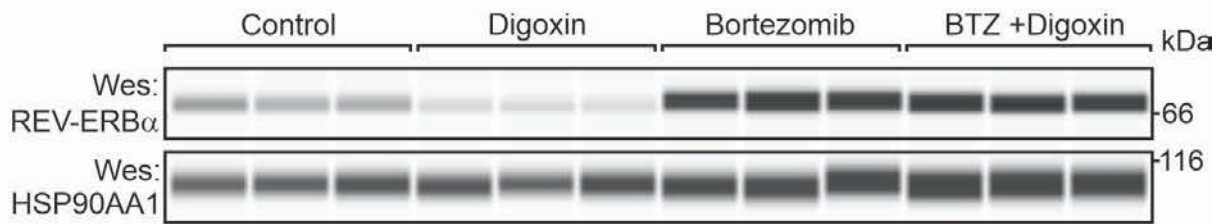






Vinod et al. - Ext. Figure 6



a**b****c****d**